The Meteoritical Society

Meteoritics & Planetary Science 54, Nr 7, 1512–1532 (2019)
doi: 10.1111/maps.13288

Cosmic ray exposure ages for ureilites—New data and a literature study

Ingo LEYA* and Peter C. STEPHENSON

Space Research and Planetology, University of Bern, Bern, Switzerland
*Corresponding author. E-mail: Ingo.Leya@space.unibe.ch

(*Received 16 March 2018; revision accepted 08 March 2019*)

Abstract–We report newly measured noble gas isotopic concentrations of He, Ne, and Ar for 21 samples from the 10 ureilites, DaG 084, DaG 319, DaG 340, Dho 132, HaH 126, JaH 422, JaH 424, Kenna, NWA 5928, and RaS 247, including the results of both single and stepwise heating extractions. Cosmic ray exposure (CRE) ages calculated using model calculations that fully account for all shielding depths and a wide range of preatmospheric radii, and are tailored to ureilite chemistry, range from 3.7 Ma for Dho 132 to 36.3 Ma for one of several measured Kenna samples. In a Ne-three-isotope plot, the data for DaG 340 and JaH 422 plot below the $Ne_{cos}/Ne_{ureilite}$ mixing envelope, possibly indicating the presence of Ne produced from solar cosmic rays. In combination with literature data and correcting for pairing, we established a fully consistent database containing 100 samples from 40 different ureilites. The CRE age histogram shows a trend of decreasing meteorite number with increasing CRE age. We speculate that the parent body of the known ureilites is moving closer to a resonance and/or that there is a loss mechanism that acts on ureilites independent of their size. In addition, there is a slight indication for a peak in the range 30 Ma, which might indicate a larger impact on the ureilite daughter body. Finally, we confirm earlier results that the majority of the studied ureilites have relatively small preatmospheric radii less or equal ~20 cm.

INTRODUCTION

With more than 470 individually classified objects, the ureilite meteorites make up the second largest group of achondrites. The known ureilites are carbon-rich ultramafic achondrites largely consisting of Mg-rich olivine and pyroxene that might represent mantle material from a single parent asteroid, the ureilite parent body (UPB) (Warren and Kallemeyn 1989; Goodrich 1992; Goodrich et al. 2004). Ureilites are subdivided into the main group, unbrecciated ureilites (formerly called monomict), and the brecciated ureilites that are polymict or dimict (Goodrich et al. 2004, 2015; Downes et al. 2008). According to recent thermal modeling and age dating, the UPB assembled < 1 Ma after CAI formation followed by partial melt segregation and crystallization no later than 5 Ma after CAI formation (Wilson et al. 2008; Goodrich et al. 2010; Amelin et al. 2015). However, some aspects of ureilites are difficult to reconcile with an igneous petrogenesis, such as variable oxygen isotope ($\Delta^{17}O$) compositions and high abundances of trapped noble gases (e.g., Clayton and Mayeda 1988; Goodrich 1992; Mittlefehldt et al. 1998). Some of the noble gases, however, might be trapped in refractory graphite and/or diamond phases (e.g., Göbel et al. 1978). All these findings make it difficult to distinguish whether ureilites represent primitive or igneous material and if they can be linked to a common source.

Considering the final steps of the UPB history, Goodrich et al. (2004) suggested that the UPB broke up early in the solar system, i.e., about 5 Ma after CAI formation, and reassembled as one or more daughter bodies (ureilite daughter body, UDB). The known ureilites are derived most likely from one of the heterogeneous brecciated UDBs (Downes et al. 2008; Herrin et al. 2010a; Warren 2012; Goodrich et al. 2015; Sanders et al. 2017). The heterogeneity is indicated by the wide variation in bulk composition, Fo content of olivine, and oxygen isotopes among the various ureilite meteorites (e.g., Clayton and Mayeda 1988; Downes et al. 2008; Warren 2012). The production and delivery

of ureilites to Earth may be a result of either a single large impact or multiple small impacts. In the first case, the ureilites should show a single cosmic ray exposure (CRE) age; in the second scenario, the CRE ages will be variable. Remember that clustering in CRE ages for the howardite–eucrite–diogenite meteorites was one of the arguments to the idea that all three meteorite types come from a single parent body (e.g., Eugster and Michel 1995).

There are important reasons to establish a consistent CRE age histogram for ureilites. However, much of the existing noble gas data for ureilites predate the development of modern cosmogenic production rate models, such as that of Leya and Masarik (2009). As such, typical data reported in the literature either omit cosmogenic production rate data and exposure ages, use older models based solely on chemical composition but without considering shielding (e.g., Mazor et al. [1970] and references therein), or use empirical models such as Eugster (1988), Aylmer et al. (1990), or Eugster and Michel (1995), which take into account both shielding (via the cosmogenic $^{22}Ne/^{21}Ne$ ratio) and chemical composition. Three recent approaches also compiled noble gas data from literature but used a constant, i.e., shielding independent ^{21}Ne production rate (Herzog and Caffee 2014; Park et al. 2014; Beard and Swindle 2017).

Here we present new noble gas data for 10 ureilites, most of which have not previously been studied for noble gases and/or CRE histories. In combination with literature data, we established a consistent database of CRE ages for 100 samples from 41 ureilites (before pairing). The CRE ages were all calculated using production rates determined using the model by Leya and Masarik (2009) assuming average chemical composition for the ureilites and fully considering the dependence of the ^{21}Ne production rates on preatmospheric radii and shielding depths. The CRE age histogram indicates a decrease, which might be an exponential, of meteorite number with increasing CRE age, indicating a continuous delivery of ureilites to Earth. Superimposed on the decrease is a slight indication for a peak in the range 30 Ma, which might be statistical significant.

EXPERIMENTAL

Sample Selection and Sample Preparation

We measured the He, Ne, and Ar isotopic concentrations of 10 ureilites. Eight ureilites are from the hot deserts of Libya (Dar al Gani "DaG" 084, DaG 319, DaG 340, and Hammadah al Hamra "HaH" 126) and Oman (Dhofar "Dho" 132, Ramlat as Sahmah "RaS" 247, Jiddat al Harasis "JaH" 422, and JaH 424). The samples from DaG 319, DaG 340, RaS 247, JaH 422, and JaH 424 were all provided by the Naturhistorisches Museum Bern/Switzerland (B. Hofmann). In addition, we studied one ureilite from Northwest Africa (NWA 5928, provided by T. Jakubowski) and we also included the ureilite Kenna in our study. Most samples are normal ureilites and ranged in weathering grade from W2 to W4. Two were petrographically distinct: DaG 319 is a polymict breccia and JaH 422 is an impact melt breccia, which makes interpreting the noble gas data likely more difficult. However, both samples were available to us and were therefore included in this study. Most of the ureilites were not studied for noble gases before. Preliminary data were reported by Cosarinsky et al. (2010).

The samples consisted of small chips almost free of fusion crust (excepting HaH 126, which contained some fusion crust). All samples were cleaned with isopropanol and dried in air. Samples for total melt extractions were in the range of 45–120 mg; samples for stepwise heating extractions ranged from 120 to 140 mg.

Noble Gas Measurements and Data Handling

Samples were prepared and measured using the same procedures and on the same spectrometers as described in detail by Huber et al. (2008). Briefly, samples were preheated in vacuum to release atmospheric gases trapped at the surface. All samples were degassed in vacuum by radio frequency induction in a Mo crucible at ~1700 °C for 35 min to extract noble gases. A second heating step at ~1750 °C confirmed complete degassing at 1700 °C. For the four samples marked "SWH" in Tables 1 and 2, a stepwise heating experiment was performed with heating steps of 600 °C, 800°C, 1000 °C, 1200 °C, 1400 °C, 1600 °C, and a final step at 1700 °C, 1740 °C, or 1800 °C. The "total" value given in Tables 1 and 2 is the sum over all temperature steps. The gases released from the samples were purified on Ti getters operated in the temperature range between room temperature and 700 °C. The He-Ne fraction was separated from the Ar fraction by trapping the latter on activated charcoals cooled to the temperature of boiling liquid nitrogen (LN_2, -196 °C). After separation, gases were further purified by Ti getters and He-Ne was measured on a sector field mass spectrometer and Ar was measured on a tandem spectrometer. Both instruments were built in-house and both are equipped with a Faraday Cup and an electron multiplier working in analog mode (see Schwarzmüller [1971] for details). Helium-Ne measurements were carried out with the spectrometer connected to a cold trap cooled with LN_2 to minimize interferences from

Table 1. Helium and Ne isotopic concentrations of 10 ureilites. Abundances are in 10^{-8} cm^3 STP g^{-1}.

Meteorite name	Temp.(°C)	^{4}He	^{4}He/^{3}He	^{20}Ne	^{20}Ne/^{22}Ne	^{21}Ne/^{22}Ne	^{21}Ne$_{cos}$	^{22}Ne/^{21}Ne$_{cos}$
Stepwise heating								
JaH 422 (SWH)	600	19.0 ± 1.0	6.44 ± 0.13	0.145 ± 0.007	2.72 ± 0.07	0.585 ± 0.020		
	800	2.67 ± 0.13	5.82 ± 0.12	0.275 ± 0.014	0.945 ± 0.020	0.723 ± 0.016		
	1000	1.85 ± 0.100	7.45 ± 0.22	0.216 ± 0.013	1.140 ± 0.058	0.689 ± 0.045		
	1200	3.69 ± 0.19	27.9 ± 1.3	0.608 ± 0.032	2.90 ± 0.16	0.639 ± 0.044		
	1400	5.13 ± 0.26	46.6 ± 3.1	0.765 ± 0.039	3.25 ± 0.12	0.593 ± 0.029		
	1600	9.86 ± 0.50	182 ± 10	1.487 ± 0.077	3.85 ± 0.12	0.547 ± 0.020		
	1700	0.436 ± 0.057	n.d.	0.184 ± 0.015	2.79 ± 0.23	0.538 ± 0.049		
	1700	0.475 ± 0.057	n.d.	0.115 ± 0.015	10.5 ± 2.5	0.074 ± 0.066		
	Total	43.1 ± 1.1	10.9 ± 0.5	3.796 ± 0.097	2.63 ± 0.10	0.619 ± 0.030	0.885	1.321
DaG 340 (SWH)	600	26.4 ± 1.3	4.61 ± 0.10	0.187 ± 0.010	2.00 ± 0.12	0.657 ± 0.062		
	800	15.2 ± 0.8	4.88 ± 0.10	0.256 ± 0.014	1.105 ± 0.039	0.786 ± 0.028		
	1000	39.3 ± 2.0	12.6 ± 0.30	1.889 ± 0.097	3.317 ± 0.093	0.566 ± 0.017		
	1200	36.7 ± 1.8	21.8 ± 0.48	2.06 ± 0.11	4.21 ± 0.12	0.506 ± 0.016		
	1400	515 ± 26	363 ± 9	27.8 ± 1.4	7.66 ± 0.17	0.257 ± 0.007		
	1600	384 ± 19	455 ± 10	16.81 ± 0.84	6.47 ± 0.14	0.329 ± 0.008		
	1700	1.68 ± 0.095	5.86 ± 0.24	1.220 ± 0.063	1.001 ± 0.027	0.761 ± 0.022		
	1800	1.00 ± 0.069	46.4 ± 4.8	0.500 ± 0.027	1.302 ± 0.045	0.746 ± 0.024		
	Total	1019 ± 32	63.0 ± 2.6	50.8 ± 1.6	5.51 ± 0.24	0.414 ± 0.019	3.681	1.277
Kenna (SWH)	600	81.6 ± 4.4	6.61 ± 0.15	0.481 ± 0.025	1.853 ± 0.049	0.819 ± 0.018		
	800	63.7 ± 3.4	6.62 ± 0.15	0.925 ± 0.048	0.873 ± 0.022	0.886 ± 0.019		
	1000	40.5 ± 2.2	7.01 ± 0.16	0.943 ± 0.050	0.864 ± 0.023	0.878 ± 0.019		
	1200	28.1 ± 1.5	10.2 ± 0.2	0.638 ± 0.033	1.078 ± 0.029	0.865 ± 0.019		
	1400	95.3 ± 5.1	26.8 ± 0.6	3.26 ± 0.17	1.150 ± 0.028	0.866 ± 0.019		
	1600	49.9 ± 2.7	13.5 ± 0.3	1.48 ± 0.13	0.977 ± 0.075	0.901 ± 0.020		
	1740	16.8 ± 0.9	7.19 ± 0.20	3.86 ± 0.23	0.819 ± 0.032	0.910 ± 0.020		
	Total	376 ± 9	9.38 ± 0.32	11.58 ± 0.33	0.960 ± 0.044	0.889 ± 0.052	10.72	1.108
RaS 247(SWH)	600	60.6 ± 3.2	5.73 ± 0.12	0.120 ± 0.004	1.087 ± 0.034	0.813 ± 0.016		
	800	35.3 ± 1.8	10.2 ± 0.2	0.382 ± 0.009	0.839 ± 0.021	0.825 ± 0.017		
	1000	63.3 ± 3.3	13.2 ± 0.3	0.886 ± 0.020	0.834 ± 0.018	0.828 ± 0.017		
	1200	16.7 ± 0.9	6.46 ± 0.14	0.353 ± 0.0083	0.812 ± 0.019	0.803 ± 0.016		
	1400	10.3 ± 0.5	6.88 ± 0.15	0.922 ± 0.021	0.849 ± 0.020	0.826 ± 0.017		
	1600	10.6 ± 0.6	7.09 ± 0.22	0.854 ± 0.021	0.863 ± 0.021	0.838 ± 0.017		
	1740	3.06 ± 0.23	5.50 ± 0.32	1.652 ± 0.036	0.830 ± 0.018	0.835 ± 0.017		
	Total	200 ± 5	8.01 ± 0.30	5.167 ± 0.052	0.843 ± 0.015	0.829 ± 0.034	5.081	1.202
Single extraction								
DaG 084	1700	93.6 ± 5.4	6.34 ± 0.15	6.19 ± 0.38	0.880 ± 0.027	0.916 ± 0.020	6.442	1.084
DaG 319	1700	448 ± 27	29.0 ± 0.6	13.06 ± 0.70	1.606 ± 0.038	0.864 ± 0.019	7.006	1.064
DaG 340-a	1700	643 ± 40	41.5 ± 0.9	30.6 ± 1.6	4.298 ± 0.097	0.510 ± 0.011	3.553	1.275
DaG 340-b	1700	1747 ± 87	127 ± 3	109.2 ± 5.6	7.80 ± 0.17	0.241 ± 0.005	3.061	1.240
Dho 132	1700	519 ± 31	166 ± 5	12.78 ± 0.82	5.55 ± 0.14	0.449 ± 0.011	0.999	1.165
HaH 126	1700	181 ± 10	9.06 ± 0.20	13.34 ± 0.71	1.461 ± 0.035	0.849 ± 0.019	7.733	1.101
JaH 422-a	1700	28.9 ± 1.7	7.45 ± 0.20	3.23 ± 0.27	2.340 ± 0.057	0.615 ± 0.013	0.8423	1.377
JaH 422-b	1700	33.4 ± 1.7	8.99 ± 0.18	3.40 ± 0.17	2.519 ± 0.055	0.604 ± 0.013	0.8080	1.373
JaH 424	1700	74.3 ± 3.8	11.5 ± 0.3	4.85 ± 0.32	1.542 ± 0.034	0.853 ± 0.017	2.676	1.086
Kenna-a	1700	325 ± 22	7.97 ± 0.19	10.08 ± 0.57	0.905 ± 0.020	0.854 ± 0.017	9.509	1.160
Kenna-b	1700	218 ± 12	7.93 ± 0.17	11.57 ± 0.61	0.939 ± 0.023	0.889 ± 0.019	10.95	1.110
Kenna-c	1700	213 ± 12	7.14 ± 0.16	12.9 ± 0.64	0.971 ± 0.023	0.871 ± 0.019	11.56	1.129
Kenna-d	1700	191 ± 11	6.91 ± 0.18	10.93 ± 0.60	0.958 ± 0.030	0.843 ± 0.029	9.613	1.169
Kenna-e	1700	217 ± 12	8.51 ± 0.18	12.15 ± 0.65	1.029 ± 0.024	0.882 ± 0.019	10.41	1.109
Kenna-f	1700	239 ± 14	9.51 ± 0.20	12.06 ± 0.68	1.104 ± 0.068	0.887 ± 0.054	9.679	1.094
NWA 5928	1700	204 ± 11	7.49 ± 0.20	9.98 ± 0.52	0.962 ± 0.020	0.884 ± 0.018	9.166	1.114
RaS 247	1700	196 ± 11	5.72 ± 0.13	8.80 ± 0.50	0.841 ± 0.026	0.863 ± 0.019	9.029	1.115

Uncertainties are 1σ. Values marked "n.d." have no data due to either (1) the reference isotope not exceeding the blank for the respective temperature step or (2) the uncertainty of the value exceeding the value itself. No uncertainties are given for the values after the component deconvolution (see text).

$H_2{}^{18}O$ and doubly charged ^{40}Ar on ^{20}Ne and from doubly charged CO_2 on ^{22}Ne. Argon was measured with the spectrometer connected to a cold trap cooled with dry ice to minimize H_2O and CO_2 background contributions. Isotope concentrations were measured in peak jumping mode.

Blank measurements were performed using the same extraction and measurement procedure as for samples. For the measurements with one gas extraction at 1700 °C, blanks were measured before and after each sample measurement. For the stepwise heating extractions, blanks were measured at 600 °C, 1000 °C, 1400 °C, and 1700 °C and interpolated linearly for the intermediate steps (800 °C, 1200 °C, 1600 °C). The blank (whether measured or interpolated) for each step was then used to correct the sample gas amounts of this respective temperature step. After measuring samples that contained large gas amounts, the crucible was degassed at 1800 °C. The blanks measured by melting the same commercial Ni foil used to wrap the samples did not differ from those measured without melting any foil. Average blank amounts are (in 10^{-10} cm^3 STP) $^4He \sim 0.1$, $^{20}Ne \sim 0.01$, and $^{40}Ar \sim 1$. The isotopic composition of the blanks was mostly atmospheric or, in the case of Ar, a mixture of air and trapped ratios. Blanks are typically in the range of less than 10% for ^4He, less than 1% for Ne isotopes but can be substantial for Ar isotopes, especially for ^{40}Ar due to extremely low ^{40}Ar concentrations in the samples.

Instrumental mass discrimination and sensitivities of the He-Ne and Ar mass spectrometers were regularly determined by analyzing calibration gases with known amounts of He, Ne, and Ar; all having atmospheric isotopic compositions, except for He, which is enriched in ^3He ($^4He/^3He \sim 100$). Since the sensitivity of the spectrometers depends on gas amounts, the data were also corrected for nonlinear behavior of the ion source and the detectors. The correction factors were empirically derived from dilution series. For most of the samples studied here the corrections are on the order of a few percent but can reach up to 12% for He and 25% for Ne for the lowest gas amounts measured in stepwise heating measurements. Note that the corrections are only for gas amounts but not for isotopic ratios.

New Data for 21 Samples from 10 Ureilites

Here we discuss the results for the 10 ureilites studied by us. We focus the discussion on the noble gas release characteristics of the stepwise heating experiments and on the determination of cosmogenic noble gas concentrations, i.e., on the correction for trapped components. The data are given in Tables 1 and 2.

Stepwise Heating Extractions

Helium: Cosmogenic $^4He/^3He$ ratios typically range between 3.5 for small meteorites and ~6 or slightly higher for larger meteorites (e.g., Alexeev 1998; Welten et al. 2003; Leya and Masarik 2009). From the data in Fig. 1 (upper panel), we can see that $^4He/^3He$ ratios are cosmogenic or close to cosmogenic for all temperature steps below 1000 °C for JaH 422, 800 °C for DaG 340, 1200 °C for Kenna, and 800 °C for RaS 247. Higher temperature steps release He with higher $^4He/^3He$ ratios, reaching 455 for the 1600 °C temperature step of DaG 340. Consequently, cosmogenic gases are released early during the stepwise pyrolysis, indicating that the radiogenic He and/or a planetary He component are both more tightly bound than the spallogenic component, which is in contrast to most stepwise heating data for other meteorite types. Most of the $^4He/^3He$ ratios are relatively low. Assuming that ^3He in ureilites is mostly cosmogenic and that most ^4He is radiogenic, the low $^4He/^3He$ ratios are consistent with low U and Th concentrations (see below) (e.g., Janssens et al. 1987; Mittlefehldt et al. 1998).

Neon: The $^{20}Ne/^{22}Ne$ ratios range between 0.819 for the 1740 °C step of Kenna and 10.5 for the second 1700 °C temperature step of JaH 422 (Fig. 1, middle panel). For Kenna and RaS 247, the $^{20}Ne/^{22}Ne$ ratios for all temperature steps are below 2 or even below 1 (for Ras 247), clearly indicating that the released Ne is dominantly cosmogenic. For JaH 422, the ratios range between 0.945 and 10.5, indicating the admixture of a trapped component. Most of the trapped gases are released at the 600 °C temperature step and above 1200 °C, while the temperature steps at 800 °C and 1000 °C release Ne with $^{20}Ne/^{22}Ne$ ratios close to cosmogenic. The release pattern is slightly different for DaG 340, the 600 °C temperature step releases some trapped gases ($^{20}Ne/^{22}Ne \sim 2$), the following step releases Ne mostly of cosmogenic origin ($^{20}Ne/^{22}Ne \sim 1$), followed by Ne with a significant trapped contribution, i.e., a $^{20}Ne/^{22}Ne$ ratio in the range 3.3–7.7. Above 1700 °C, i.e., close to the final degassing temperature, the $^{20}Ne/^{22}Ne$ ratio is again close to cosmogenic. Since many of the Dar al Gani ureilites are polymict, DaG 340 might be a single clast from a polymict ureilite and might therefore contain additional and/or other trapped Ne components, which would explain why the release pattern for DaG 340 differs from that of the other studied samples.

Argon: Figure 1 (lower panel) depicts for the four ureilites studied via stepwise heating techniques the $^{38}Ar/^{36}Ar$ ratios for all temperature steps. The ratios for JaH 422 vary in the small range from 0.183 to 0.196, clearly indicating that the released Ar is dominated by a planetary component (also indicated by the low

Table 2. Argon isotopic concentrations of 10 ureilites. Abundances are in 10^{-8} cm^3 STP g^{-1}.

Meteorite name	Temp.(°C)	^{36}Ar	^{40}Ar/^{36}Ar	^{38}Ar/^{36}Ar
Stepwise heating				
JaH 422 (SWH)	600	11.1 ± 0.6	17.50 ± 0.40	0.1843 ± 0.0042
	800	16.1 ± 0.9	1.336 ± 0.042	0.1881 ± 0.0043
	1000	56.1 ± 3.2	0.266 ± 0.010	0.1890 ± 0.0043
	1200	268 ± 15	0.0213 ± 0.0018	0.1870 ± 0.0042
	1400	307 ± 18	0.0027 ± 0.0018	0.1874 ± 0.0042
	1600	676 ± 39	0.00162 ± 0.00045	0.1868 ± 0.0042
	1700	1.1 ± 0.1	2.14 ± 0.43	0.191 ± 0.025
	1700	0.4 ± 0.1	1.1 ± 1.0	0.196 ± 0.063
	Total	1336 ± 45	0.1507 ± 0.0081	0.1871 ± 0.0093
DaG 340 (SWH)	600	3.6 ± 0.2	48.9 ± 1.1	0.2019 ± 0.0065
	800	3.4 ± 0.2	1.752 ± 0.077	0.1898 ± 0.0057
	1000	82.3 ± 4.7	0.0586 ± 0.0040	0.1873 ± 0.0043
	1200	119 ± 6.8	0.0212 ± 0.0027	0.1863 ± 0.0043
	1400	1698 ± 97	0.00103 ± 0.00077	0.1859 ± 0.0042
	1600	2063 ± 118	0.00032 ± 0.00029	0.1860 ± 0.0042
	1700	3.5 ± 0.2	n.d.	0.211 ± 0.010
	1800	2.0 ± 0.2	0.56 ± 0.21	0.186 ± 0.016
	Total	3975 ± 153	0.0402 ± 0.0025	0.186 ± 0.011
Kenna (SWH)	600	3.3 ± 0.5	139 ± 22	0.1975 ± 0.0041
	800	4.2 ± 0.6	1.11 ± 0.18	0.1990 ± 0.0042
	1000	4.0 ± 0.6	0.536 ± 0.086	0.2006 ± 0.0042
	1200	9.9 ± 1.4	0.099 ± 0.016	0.1998 ± 0.0041
	1400	51.1 ± 7.2	0.0311 ± 0.0050	0.2408 ± 0.0049
	1600	33.7 ± 4.8	0.0190 ± 0.0031	0.1986 ± 0.0042
	1740	0.28 ± 0.04	18.6 ± 3.0	0.644 ± 0.014
	Total	106 ± 9	4.42 ± 0.49	0.199 ± 0.024
RaS 247 (SWH)	600	0.35 ± 0.02	120.7 ± 8.8	0.2023 ± 0.0045
	800	0.24 ± 0.01	61.8 ± 4.5	0.2116 ± 0.0049
	1000	1.5 ± 0.1	2.47 ± 0.18	0.2035 ± 0.0043
	1200	0.93 ± 0.05	0.919 ± 0.067	0.2234 ± 0.0048
	1400	9.9 ± 0.5	0.216 ± 0.016	0.2168 ± 0.0044
	1600	14.9 ± 0.8	0.0685 ± 0.0050	0.2018 ± 0.0041
	1740	0.52 ± 0.3	4.24 ± 0.31	0.3889 ± 0.0082
	Total	28.4 ± 0.9	2.38 ± 0.11	0.1995 ± 0.0093
Single extractions				
DaG 084		6.1 ± 0.3	252.5 ± 5.1	0.2471 ± 0.0049
DaG 319		889 ± 44	0.585 ± 0.012	0.1903 ± 0.0038
DaG 340-a		2116 ± 106	0.0387 ± 0.0014	0.1927 ± 0.0071
DaG 340-b		8822 ± 441	0.0153 ± 0.0003	0.1789 ± 0.0038
Dho 132		2299 ± 115	0.0771 ± 0.0029	0.1930 ± 0.0072
HaH 126		1343 ± 67	0.0896 ± 0.0033	0.1935 ± 0.0072
JaH 422-a		521 ± 26	0.3222 ± 0.0071	0.1866 ± 0.0041
JaH 422-b		1013 ± 51	0.3085 ± 0.0065	0.1802 ± 0.0038
JaH 424		338 ± 17	0.943 ± 0.021	0.1867 ± 0.0041
Kenna-a		85.2 ± 6.1	6.62 ± 0.63	0.1988 ± 0.0040
Kenna-b		106 ± 5.3	6.75 ± 0.14	0.1949 ± 0.0039
Kenna-c		86.7 ± 4.3	1.81 ± 0.04	0.1964 ± 0.010
Kenna-d		65.5 ± 3.3	5.19 ± 0.10	0.2006 ± 0.0040
Kenna-e		120 ± 6.0	6.30 ± 0.13	0.1939 ± 0.0039
Kenna-f		n.d.	n.d.	n.d.
NWA 5928		74.1 ± 3.7	4.62 ± 0.10	0.1930 ± 0.0043
RaS 247		36.1 ± 5.1	3.80 ± 0.61	0.2153 ± 0.0045

Uncertainties are 1σ. Values marked "n.d." have no data due to either (1) the reference isotope not exceeding the blank for the respective temperature step or (2) the uncertainty of the value exceeding the value itself.

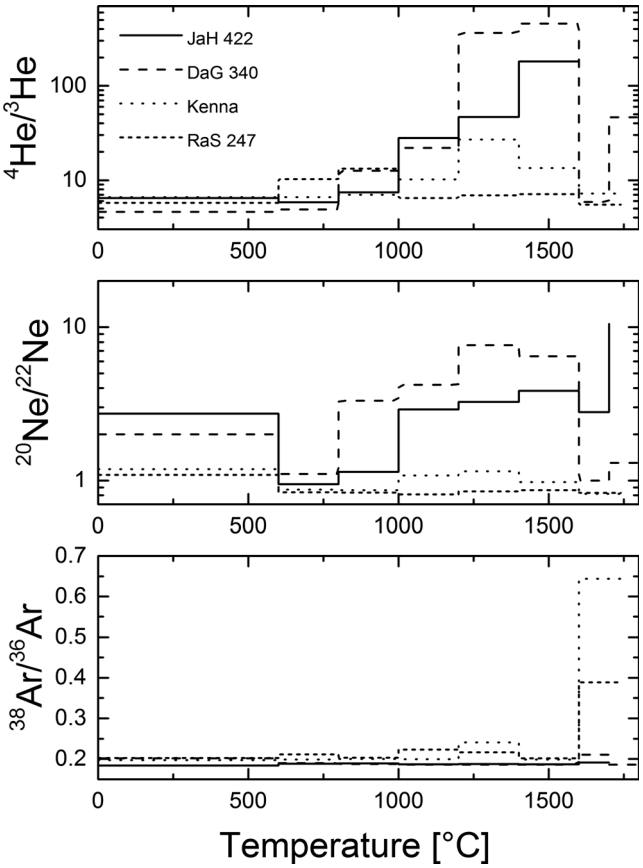

Fig. 1. ^{4}He/^{3}He, ^{20}Ne/^{22}Ne, and ^{38}Ar/^{36}Ar ratios as a function of release temperature for JaH 422, DaG 340, Kenna, and RaS 247. For more information, see text.

^{40}Ar/^{36}Ar ratios). The two extractions at 1700 °C have slightly higher ^{38}Ar/^{36}Ar ratios, indicating a slighter higher, though still small, contribution of cosmogenic Ar. The same trends are visible for DaG 340 and Kenna, though the ratios vary slightly more with release temperature. All three ureilites, however, have ^{38}Ar/^{36}Ar ratios below 0.2, clearly indicating that the released Ar is predominantly trapped. The ureilite RaS 247 has a slightly different release characteristic, as the ^{38}Ar/^{36}Ar ratios vary between 0.2 and 0.38, indicating a slightly higher contribution of cosmogenic Ar, though trapped Ar is still dominant.

Single Extractions and Totals of Stepwise Heating Extractions

Helium: The measured ^{4}He/^{3}He ratios vary between ~6 for DaG 084 and ~166 for Dho 132. The majority of the data are below 10, clearly indicating that contributions of radiogenic and/or planetary ^{4}He are low. Assuming that all ^{3}He is cosmogenic and that the cosmogenic ^{4}He/^{3}He ratio is 5.72, i.e., given by the lowest measured ^{4}He/^{3}He ratio, we can calculate the amount of radiogenic and/or planetary ^{4}He for each meteorite. However, we start the discussion with cosmogenic ^{3}He. The reproducibility of the ^{3}He concentrations for the three DaG 340 and JaH 422 samples is reasonable; the maximum differences are 18% and 6%, respectively. The situation for Kenna is different; the ^{3}He concentrations for the seven analyzed samples vary by more than 60%, which is much more than the experimental reproducibility (about 10%) that we routinely checked using a homogeneous sample powder from the meteorite Millbillilillie. For RaS 247, the differences between the two samples, one measured by stepwise heating and one by one step pyrolysis, are 37%, i.e., also higher than the experimental reproducibility. We might speculate that part of the bad reproducibility is caused by an inhomogeneous chemical composition. However, varying the carbon concentration between zero and 10% changes the ^{3}He concentration only by about 10% (based on model calculations by Leya and Masarik 2009), i.e., not enough to fully account for the observed variation.

A comparison of our results to the few data found in literature reveals some serious discrepancies. The new ^{3}He concentrations for DaG 084 are more than a factor of ~2 lower than the value given by Scherer et al. (2000). A similar observation holds for DaG 319: the value by Scherer et al. (1998) is more than a factor of ~2.5 higher than ours. For DaG 340, all three of our data are lower by a factor of 1.8 than the value given by Scherer et al. (1998). For Kenna, the results are contradictory: the data by Göbel et al. (1978) and Wilkening and Marti (1976) are in the range (62–74) $\times$ 10^{-8} cm^3 STP g^{-1}, whereas our measurements give values in the range (25–40) $\times$ 10^{-8}cm^3 STP g^{-1}, i.e., substantially lower.

The difficulty with the ^{3}He data can best be seen in Fig. 2 in which we plot $(^3\text{He}/^{21}\text{Ne})_{cos}$ as a function of $(^{22}\text{Ne}/^{21}\text{Ne})_{cos}$ for the studied ureilites together with literature data and results from the model calculations discussed further below. Also shown is the empirical correlation by Nishiizumi et al. (1980) that is based on data from 138 chondrites. Three important trends are visible. First, the modeled trend differs from the empirical correlation especially for low $(^{22}\text{Ne}/^{21}\text{Ne})_{cos}$ ratios. This finding either indicates that the empirical correlation deduced for chondrites is not applicable to ureilites and/or that the model fails in describing production rates for small ureilites. Second, all of our data as well as most of the literature fall below both the model predictions and the empirical correlation line (Nishiizumi et al. 1980). Third, the experimental data scatter widely, showing no visible trend of $(^3\text{He}/^{21}\text{N})_{cos}$ as a function of $(^{22}\text{Ne}/^{21}\text{Ne})_{cos}$. Especially important is thereby the finding that also data from one ureilite scatter significantly, indicating large sample-to-sample

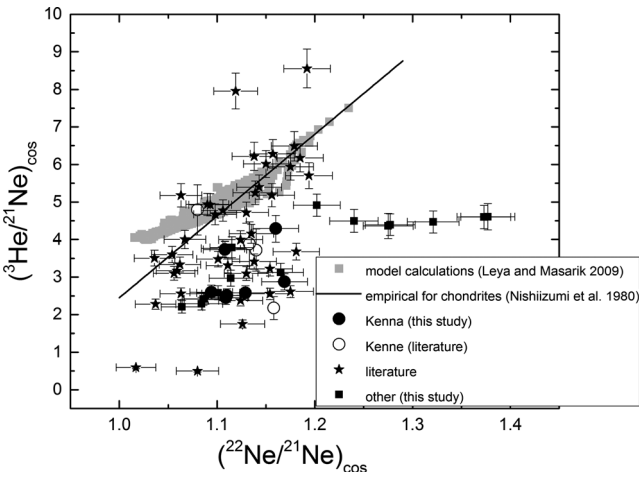

Fig. 2. $(^3He/^{21}Ne)_{cos}$ as a function of $(^{22}Ne/^{21}Ne)_{cos}$ for the studied ureilites and literature data. Almost all experimental data plot below the model predictions and the empirical correlation line (Nishiizumi et al. 1980) indicating that almost all ureilites experienced ^3He deficits.

heterogeneities. As an example we discuss the data from Kenna. The data from our study are shown by solid black dots and the literature data (Wilkening and Marti 1976; Okazaki et al. 2003; Rai et al. 2003) are shown by open dots. While the $(^{22}Ne/^{21}Ne)_{cos}$ ratios vary slightly more than expected considering the experimental uncertainties (1σ standard deviation: 2–3%), the maximum deviation for the $(^3He/^{21}Ne)_{cos}$ ratios is ~75% with a standard deviation of the mean of ~20%. Consequently, while the reproducibility of the $(^{22}Ne/^{21}Ne)_{cos}$ ratio is reasonable, the variation of $(^3He/^{21}Ne)_{cos}$ is far too large to be caused by analytical artifacts. Note that we can for our samples exclude ^3He losses caused by sample preparation because all samples were treated similarly (same preheating temperature, same duration of preheating, similar vacuum conditions) and we regularly checked the noble gas extraction and cleaning procedures using calibration gases and standard meteorites. It can be seen that the literature data (open symbols, Okazaki et al. 2003; Rai et al. 2003; Wilkening and Marti 1976) show the same trend as our data, they plot into the same field far below the model predictions and the empirical correlation line, also indicating substantial and highly variable ^3He deficits. Consequently, while our data at first glance indicate to be highly variable and therefore unreliable they are fully consistent with literature data. Therefore, the significant scatter most likely rather indicates an inherent feature of the ureilites that is worth being studied in more detail (see below).

The second important feature in Fig. 2 is that most of the experimental data (shown a solid black stars) scatter widely below the model predictions and/or the empirical correlation line, indicating that most ureilites show variable ^3He deficits relative to what is expected. This finding indicates that most of the $^3He_{cos}$ concentrations published for ureilites might be too low due to ^3H and/or ^3He diffusive losses. Since in this study we are interested in reliable CRE ages for ureilites, we concentrate on $^{21}Ne_{cos}$, which we consider as more reliable than $^3He_{cos}$. Note that it would be worth studying in more detail if and why ^3He deficits seem to be more common in ureilites than in other chondrite types.

With the assumed cosmogenic $(^4He/^3He)_{cos}$ ratio of 5.72, we calculated excess ^4He and assumed all of it to be radiogenic, i.e., $^4He_{rad}$. Considering that ^3He is most likely too low due to ^3He losses, this procedure likely overestimates $^4He_{rad}$. Furthermore, assuming all excess ^4He to be radiogenic also overestimates $^4He_{rad}$ because contributions from planetary ^4He are expected. The $^4He_{rad}$ concentrations vary between zero for RaS 247 and DaG 084 to ~1700 × 10^{-8} cm^3 STP g^{-1} for one sample of DaG 340; they also vary significantly for different samples from the same meteorite. For example, the $^4He_{rad}$ concentrations vary by a factor of ~3 for the three DaG 340 samples, by a factor of ~3 for the three JaH 422 samples, and by more than a factor of ~4 for the seven Kenna samples. Assuming U and Th concentrations of 1 ng/g and 3 ng/g, respectively (cf. Mittlefehldt et al. 1998), we calculate ^4He gas retention ages ranging from zero to an unreasonably high apparent age of 8100 Ma. For 6 of the 21 samples, we calculate apparent ages older than the age of the solar system. With U and Th concentrations of 1 and 3 ng g^{-1}, respectively, we calculate a maximum possible $^4He_{rad}$ concentration of 155 × 10^{-8} cm^3 STP g^{-1}. Consequently, higher $^4He_{rad}$ concentrations are only possible for higher U and Th concentrations. Turning the argument around, a $^4He_{rad}$ concentration as high as 1700 × 10^{-8} cm^3 STP g^{-1} measured for one DaG 340 sample requires U and Th concentrations in the range 10 and 30 ng/g, i.e., much higher than usually measured in ureilites (Mittlefehldt et al. 1989). Note that Janssens et al. (1987) measured for one ureilite (Dylapur) a high U concentration of almost 7 ng g^{-1}, i.e., much higher than the average. It is unlikely that most of the ureilites studied by us have such exceptionally high U and Th concentrations, especially if we consider that Janssens et al. (1987) measured for other ureilites U concentrations in accord with low values in the range 1 ng g^{-1}. We therefore conclude that some of the studied ureilites contain substantial amounts of trapped ureilite He with $^3He/^4He$ ratios likely similar to Q-He, i.e., $^3He/^4He \sim 10^{-4}$. However, a deconvolution of the measured data into spallogenic, radiogenic, and planetary components is not possible.

Neon: Figure 3 depicts the Ne data in a Ne-three-isotope plot. In addition to the data for the single

temperature step extractions, we also plot the data from the stepwise heating extractions, which helps to better determine the mixing line(s) and to better correct for trapped components. We also plot the Ne endmember composition for ureilite gases (index "ureilite"), which has a $^{20}Ne/^{22}Ne$ ratio of either 10.4 (Ott et al. 1985) or 10.7 (Göbel et al. 1978; Busemann et al. 2000). The ratio $(^{21}Ne/^{22}Ne)_{ureilite}$ is not well known. Here we assume $(^{21}Ne/^{22}Ne)_{ureilite} = 0.031$ (e.g., Busemann et al. 2000). All data plot on a mixing line between cosmogenic Ne and a trapped component, which is most likely $Ne_{ureilite}$. The two dashed lines are drawn to cover all data using $Ne_{ureilite}$ as one endmember, i.e., both lines start at $Ne_{ureilite}$. Doing so, the cosmogenic $^{21}Ne/^{22}Ne$ ratio (index "cos") at $(^{20}Ne/^{22}Ne)_{cos} = 0.87$ varies between 0.73 and 0.92, which is lower than the average ratio for most chondrite types. For the determination of $^{21}Ne_{cos}$ and $(^{22}Ne/^{21}Ne)_{cos}$, we use a standard two-component deconvolution with $(^{20}Ne/^{22}Ne)_{ureilite} = 10.4$ (Ott et al. 1985) and $(^{20}Ne/^{22}Ne)_{cos} = 0.84$, which is the lowest ratio measured in this study for a bulk sample (RaS 247, both total of stepwise heating and single temperature extraction). The results for $^{21}Ne_{cos}$ and $(^{22}Ne/^{21}Ne)_{cos}$ vary only very little with our choice for the $Ne_{ureilite}$ endmember, i.e., 10.7 (Göbel et al. 1978; Busemann et al. 2000) or 10.4 (Ott et al. 1985). The $^{21}Ne_{cos}$ concentrations determined in this study vary between 0.8×10^{-8} cm^3 STP g^{-1} and 11.6×10^{-8} cm^3 STP g^{-1} (Table 1). The reproducibility of the $^{21}Ne_{cos}$ concentrations for samples that have been measured more than once is usually within or at least close to the uncertainties. For example, the standard deviations of the mean $^{21}Ne_{cos}$ concentrations are 3.5%, 7.8%, and 7.0% for JaH 422, DaG 340, and Kenna, respectively. The only exception is RaS 247, for which $^{21}Ne_{cos}$ of the two samples varies by almost a factor of two. The reproducibility of $(^{22}Ne/^{21}Ne)_{cos}$, which for all studied samples range from 1.064 to 1.377, is slightly larger than the experimental uncertainties, the variation is less than 4% for the different JaH 422 samples and less than 3% for the three DaG 340 samples. For the seven Kenna and two RaS 247 samples, the maximum variation in $(^{22}Ne/^{21}Ne)_{cos}$ is ~7%. Interestingly, despite variable $(^{22}Ne/^{21}Ne)_{cos}$ ratios for the different aliquots of the same meteorite, the deduced CRE ages usually agree within the uncertainties (see below).

Argon: The Ar isotopic concentrations are given in Table 2. The $^{40}Ar/^{36}Ar$ ratios range from 0.0153 for one of the DaG 340 samples to 252.5 for DaG 084. Excluding the exceptionally high value for DaG 084, the measured range for $^{40}Ar/^{36}Ar$ reduces to 0.0153–6.75; the average ratio is 2.34 ± 2.56. The lowest $^{40}Ar/^{36}Ar$ ratio measured so far in ureilites is $(2.9 \times 1.7) \times 10^{-4}$ (Göbel et al. 1978). Considering that ureilites have K concentrations in the range 15 ppm (e.g., Scherer et al. 1998), less than 120×10^{-8} cm^3 STP g^{-1} radiogenic ^{40}K can have been produced over the last 4.5 Ga. Consequently, only for RaS 247 (stepwise heating) and DaG 340-a can the measured ^{40}Ar fully be explained by radiogenic contributions; the higher concentrations measured for all other samples must be due to atmospheric contamination. Note that most of the studied ureilites are from hot deserts. Correcting the Ar data for atmospheric contamination by assuming all ^{40}Ar to be atmospheric gives $^{38}Ar/^{36}Ar$ ratios in the range 0.177–0.203, clearly indicating a primordial rather than a cosmogenic origin. The data indicate that $(^{38}Ar/^{36}Ar)_{ureilite}$ must be lower than 0.177, which is the lowest ratio determined by us. However, since this Ar fraction must contain a cosmogenic contribution with a $^{38}Ar/^{36}Ar$ ratios close to 1.5, the ureilitic $^{38}Ar/^{36}Ar$ ratio must be even lower than 0.177. Note that it is usually assumed that $(^{38}Ar/^{36}Ar)_{ureilite} = 0.190$ (e.g., Göbel et al. 1978; Busemann et al. 2000).

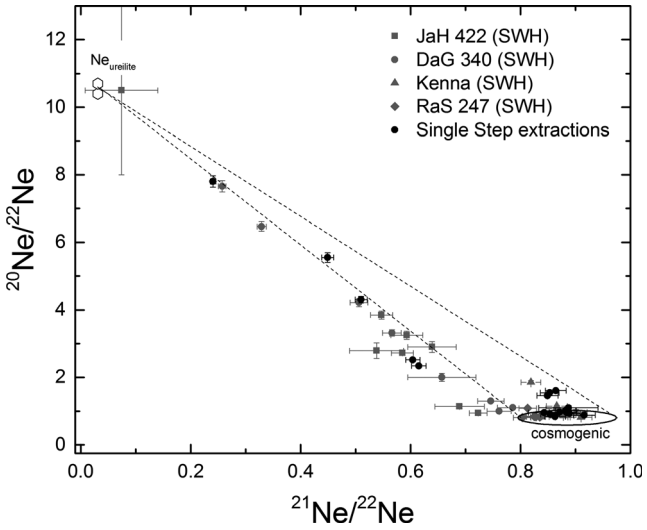

Fig. 3. Ne-three-isotope plot for the stepwise heating extractions (label SWH) of JaH 422, DaG 340, Kenna, and RaS 247. Also shown are the data for the single temperature step extractions of DaG 084, DaG 319, DaG 340, Dho 132, HaH 126, JaH 422, JaH 424, Kenna, NWA 5928, and RaS 247. For more information, see text.

CHEMICAL COMPOSITION AND PRODUCTION RATE SYSTEMATICS

The production rate of a cosmogenic nuclide, e.g., $^{21}Ne_c$, depends on the radius of the meteoroid in space, the depth of the sample within the preatmospheric object (radius and depth are usually merged together into the term shielding depth), the geometry of the

meteoroid in space, the chemical composition of the meteoroid, and the chemical composition of the studied sample (e.g., Leya and Masarik 2009). Since the shielding conditions are very often not known most studies rely on correlations as the one discussed further below.

We first discuss the bulk chemical composition. We collected bulk chemistry data of 36 samples from 26 ureilites from various literature sources. The results are compiled in Table 3 where we also give the average chemical composition used for the model calculations (see below). The overall relative deviation from the mean is modest, with the relative 1σ standard error of the mean for major elements (those with ≥10% of the total mass, i.e., O, Mg, Si, and Fe) ranging between 1.1% and 3.6%. For minor elements (those with ≤10% of the total mass, i.e., Na, Al, S, Ca, K, Ti, Mn, and Ni), the relative 1σ standard error of the mean ranges between 1.8% and 16.3%. The result compiled by us is in excellent agreement with the average elemental composition given by Rai et al. (2003), which is based on nine ureilites.

Based on the determined average chemical composition, we calculated ^{21}Ne and ^{22}Ne production rates as a function of preatmospheric radius and shielding depth using the model from Leya and Masarik (2009). Briefly, the model is based on the spectra of primary and secondary particles calculated using Monte-Carlo techniques and the cross sections for all relevant nuclear reactions. The current version of the model only distinguishes particle spectra for ordinary chondrites, carbonaceous chondrites, and iron meteorites. This, however, is not a serious limitation. The particle spectra depend, beside radius and shielding depth, on the bulk chemical composition of the entire meteoroid but not, or only very little, on the chemical composition of an individual sample. As an example, for calculating the cosmogenic nuclide production rates for a metal inclusion in an ordinary chondrite one has to use the particle spectra for ordinary chondrites but considering only nuclear reactions relevant for this metal inclusion. Therefore, the particle spectra for ordinary chondrites not only cover bulk samples but also all inclusions and/or mineral separates in ordinary chondrites. In addition, the dependence of the particle spectra on the bulk chemical composition of a meteorite is relatively minor; i.e., the particle spectra for H-, L-, and LL-chondrites are essentially indistinguishable. Here we use the model for carbonaceous chondrites because carbonaceous chondrites are a better match for ureilites than ordinary chondrites due to their more similar metal and carbon content. Since the production rates depend on preatmospheric radius of the meteoroid and shielding depth of the sample, two parameters usually not known, we cannot use the modeled results directly but rather rely on production rate systematics. We therefore calculated ^{21}Ne production rates, P21, as a function of $(^{22}Ne/^{21}Ne)_{cos}$. The production rates have been calculated using the particle spectra for all shielding depths in carbonaceous chondrites with preatmospheric radii less or equal 100 cm and using the average chemical composition given in Table 3. The modeled results indicate that small meteorites have high $(^{22}Ne/^{21}Ne)_{cos}$ ratios and relatively low P21 values in the range 0.2×10^{-8} cm^3 STP g^{-1} Ma^{-1}. The larger the meteorite, the smaller the $(^{22}Ne/^{21}Ne)_{cos}$ ratios and the larger P21. Plotting the data for all shielding depths gives a correlation close to linear. As it is very often in CRE age studies, we not try to calculate preatmospheric radii for all studied ureilites and the shielding depths for each studied sample because this is very often not possible with the limited data available. We instead use the modeled data and calculated a linear fit of P21 values as a function of $(^{22}Ne/^{21}Ne)_{cos}$. In addition to the fitted linear correlation, we also show in Fig. 4 estimated uncertainties for the modeled P21, which we assume is 15%. From Fig. 4, three important points must be emphasized. First, the linear correlation cannot be used outside the range of $(^{22}Ne/^{21}Ne)_{cos}$ ratios given by the model, which is 1.016–1.235. Second, the model clearly demonstrates that P21 depends on shielding. For example, the $(^{22}Ne/^{21}Ne)_{cos}$ ratios for all samples studied here range from 1.017 to 1.231, which gives P21 values in the range 0.171×10^{-8} cm^3 STP g^{-1} Ma^{-1} and 0.494×10^{-8} cm^3 STP g^{-1} Ma^{-1}, i.e., they vary by almost a factor of three. The $(^{22}Ne/^{21}Ne)_{cos}$ ratios in our data set vary by more than 20%, which is more than the 10% variation in the data set by Beard and Swindle (2017). These authors argued that the variation in $(^{22}Ne/^{21}Ne)_{cos}$ ratios results in a 15% variation of the $^{21}Ne_{cos}$ production rates. In contrast, the model used here predicts for 10% $(^{22}Ne/^{21}Ne)_{cos}$ variations $^{21}Ne_{cos}$ production rate variations of almost 45%, i.e., slightly higher. In the other study of ureilite CRE ages, Herzog and Caffee (2014) used a constant $^{21}Ne_{cos}$ production rate of 0.421×10^{-8} cm^3 STP g^{-1} Ma^{-1}. While this value is well within the range predicted by the model calculations, it is slightly biased to larger preatmospheric radii. Averaging all $^{21}Ne_{cos}$ production rates used by us gives a value of 0.316×10^{-8} cm^3 STP g^{-1} Ma^{-1} with a standard deviation of about 25%, i.e., slightly lower that the value used by Herzog and Caffee (2014). Anyway, from the model predictions, we conclude that $^{21}Ne_{cos}$ production rates are shielding dependent and that this shielding dependency must be taken into account. Third, the established correlation between P21 and $(^{22}Ne/^{21}Ne)_{cos}$ only slightly depends on the chemical composition. The

Table 3. Concentrations of major and minor elements relevant to this work. Blank cells indicate that no relevant data were available in the respective reference. All data are reported as wt%.

Meteorite name	Reference	O	Na	Mg	Al	Si	S	Ca	K	Ti	Mn	Fe	Ni
A-881931	Yanai et al. (1995)	43.39	0.16	21.26	0.27	17.62	0.32	0.96	0.02	0.02	0.25	15.65	0.11
ALHA77257	Rai et al. (2003), Takeda (1987)	45.14	0.02	23.92	0.05	19.22	0.00	0.76	0.01	0.02	0.29	10.55	
ALHA77257	Yanai et al. (1995)	43.66	0.01	25.36	0.11	18.72	0.12	0.61	0.02	0.04	0.30	11.18	0.08
ALHA78019	Yanai et al. (1995)	42.96	0.10	21.59	0.10	16.07	0.64	0.71	0.04	0.05	0.31	17.25	0.18
Almahatta Sitta (AS#1)	Welten et al. (2010)	37.00		19.60	0.16	19.00		0.92			0.28	20.80	0.37
Almahatta Sitta (AS#4)	Welten et al. (2010)	42.00		20.90	0.29	22.00		1.72			0.38	9.70	0.05
Almahatta Sitta (AS#7)	Friedrich et al. (2010)									0.03	0.31		
Almahatta Sitta (AS#4)	Friedrich et al. (2010)		0.03	24.50	0.26			1.05		0.02	0.37	10.70	0.06
Almahatta Sitta (AS#15)	Friedrich et al. (2010)		0.08	20.90	0.48			4.23		0.07	0.37	9.99	0.08
Almahatta Sitta (AS#47)	Friedrich et al. (2010)		0.03	21.10	0.15			0.87		0.01	0.27	16.30	0.19
Almahatta Sitta (AS#15)	Welten et al. (2010)	39.00		17.00	0.43	20.00		5.75			0.32	15.20	0.14
Almahatta Sitta (AS#36)	Welten et al. (2010)	43.00		23.70	0.17	21.00		1.12			0.31	7.60	0.03
Almahatta Sitta (AS#44)	Welten et al. (2010)	40.00		19.50	0.28	21.00		1.73			0.30	14.60	0.16
Almahatta Sitta (AS#47)	Welten et al. (2010)	40.00		20.10	0.14	21.00		1.05			0.28	15.10	0.17
Dingo Pup Donga	Vdovykin (1976), McCall and Cleverly (1968)	42.08	0.04	18.21	0.18	17.85	0.33	1.01	0.02	0.05	0.26	15.64	0.23
Dyalpur	Vdovykin (1976), Wiik (1969)	39.62	0.06	23.46	0.17	19.57	0.63	0.97		0.11	0.31	11.31	0.13
EET 83309	Rai et al. (2003), Warren and Kallemeyn (1989)		0.12	21.70	0.33	18.6	0.33	0.89	0.02	0.07	0.29	13.90	0.18
Goalpara	Vdovykin (1976), Wiik (1969)	38.35	0.05	22.02	0.47	19.06	0.61	0.31		0.07	0.31	16.40	0.09
Haverö	Vdovykin (1976), Wiik (1972)	39.50	0.03	23.49	0.14	18.80	0.19	0.08	0.01	0.04	0.29	14.94	0.12
JaH 422	Janots et al. (2011)		0.04	21.47	0.10	16.85		1.59	0.01	0.02	0.28	13.47	0.20
JaH 424	Janots et al. (2011)		0.05	20.29	0.17	18.32		1.18	0.04	0.01	0.30	14.91	0.21
Jalanash	Yanai et al. (1995)	41.46	0.07	23.08	0.46	18.41	0.28	0.59	0.02	0.05	0.37	15.14	0.09
Kenna	Boynton et al. (1976)	42.21	0.02	19.96	0.12	20.29	0.00	0.93		0.12	0.28	15.93	0.12
Lahrauli	Vdovykin (1976), Bhandari et al. (1981)	40.61	0.11	21.80	0.70	18.23	0.11	1.49		0.06	0.29	15.49	0.12
MET 78008	Yanai et al. (1995)	42.64	0.15	20.42	0.41	17.92	0.18	2.25	0.02	0.08	0.30	15.63	0.25
Nilpena	Jaques and Fitzgerald (1982)		0.08	19.50	0.28	18.39	0.27	0.96	0.03	0.02	0.24	15.99	0.20
North Haig	Vdovykin (1976), McCall and Cleverly (1968)	41.37	0.06	20.81	0.09	17.20	0.36	0.90	0.02	0.05	0.29	13.73	0.11
Novo-Urei	Vdovykin (1976), Wiik (1969)	38.69	0.05	22.23	0.26	18.57	0.58	0.57	0.03	0.08	0.31	15.64	0.12
PCA 82506	Jarosewich (1990)	44.64	0.02	21.03	0.05	18.87	0.01	0.69	0.01	0.02	0.30	14.21	0.08
RaS 247	Janots et al. (2011)		0.06	20.26	0.23	18.53		1.16	0.01	0.02	0.30	14.88	0.19
Roosevelt County 027	Goodrich et al. (1987)		0.02	22.07	0.21	18.51		0.86	0.00	0.12	0.29	16.17	0.00
Y 74123	Takeda (1987), Yanai et al. (1995)			22.49	0.48	15.52	0.30	0.39	0.02	0.05	0.29	16.33	0.14
Y 74130	Takeda (1987), Yanai et al. (1995)			19.50	0.44	19.69	0.15	1.42	0.02	0.07	0.27	13.55	0.12
Y 74659	Takeda (1987), Yanai et al. (1995)			23.39	0.57	20.06	0.18	1.22	0.02	0.08	0.33	8.20	0.14
Y 790981	Takeda (1987), Yanai et al. (1995)			20.79	0.28	17.11	0.71	0.71	0.02	0.07	0.27	15.39	0.21
Y 791538	Takeda (1987), Yanai et al. (1995)		0.07	23.06	0.58	20.31	0.19	1.34	0.03	0.05	0.30	7.43	0.09
Average ("typical")	This work	41.30	0.06	21.44	0.27	18.83	0.30	1.23	0.02	0.05	0.30	13.97	0.14

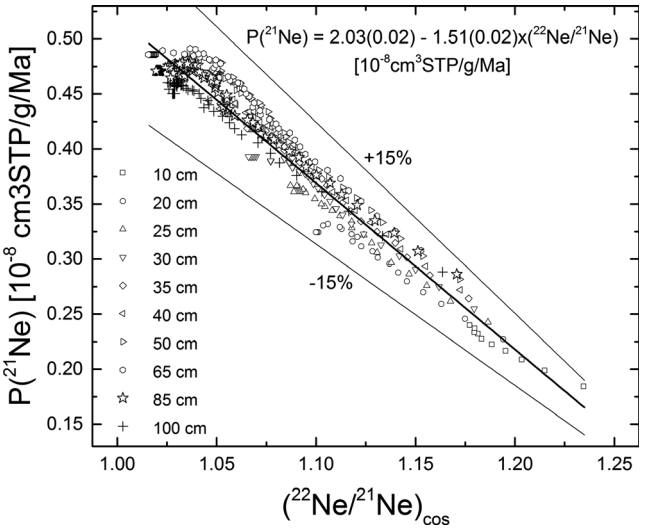

Fig. 4. Modeled ^{21}Ne production rates as a function of $(^{22}Ne/^{21}Ne)_{cos}$ ratios for ureilites with preatmospheric radii less or equal 100 cm. For the model calculations, we use the particle spectra for carbonaceous chondrites but used the average chemical composition for ureilites. There is a linear dependence of ^{21}Ne production rates as a function of $(^{22}Ne/^{21}Ne)_{cos}$ ratios.

average chemical composition given in Table 3 corresponds to a Fo number of 78, which is at the lower edge of Fo numbers for ureilites (ranging from 75 to 92). However, reducing the Fe content to a Fo number of 92 increases the production rates only by ~20%. Since most of the studied ureilites have Fo numbers in the relatively narrow range from 75 to 80, we conclude that using an average chemical composition with Fo number 78 is well applicable for calculating the $^{21}Ne_{cos}$ production rates for ureilites. Note that Downes et al. (2008) also argued that ureilitic olivine clast with magnesium numbers less than 85 are much more common than those with magnesium numbers larger than 85.

RESULTS—COSMIC RAY EXPOSURE AGES

New Measured Data

The $(^{22}Ne/^{21}Ne)_{cos}$ ratios after the component deconvolution are summarized in Table 1. As discussed before, the model predicts for ureilites with preatmospheric radii lower than or equal to 100 cm and having average chemical composition (Table 3) $(^{22}Ne/^{21}Ne)_{cos}$ ratios between 1.016 and 1.235. Ratios higher or lower than this can be due to (1) a wrong assumption of the trapped component(s) used for the component deconvolution, (2) a wrong assumption of the chemical composition used for modeling, (3) errors in the assumed $(^{20}Ne/^{22}Ne)_{cos}$ ratio used for the component deconvolution, or (4) errors in the modeling calculations. From the 10 studied ureilites, eight have—after the component deconvolution using $Ne_{ureilite}$ as the endmember—$(^{22}Ne/^{21}Ne)_{cos}$ ratios well within the range defined by the model; only the three samples from DaG 340 and JaH 422 have higher ratios. Changing the trapped component does not solve the problem with the model disagreement. If we assume for the component deconvolution that measured Ne is a mixture of atmospheric contamination and cosmogenic Ne instead of a mixture of $Ne_{ureilite}$ and cosmogenic Ne, the $(^{22}Ne/^{21}Ne)_{cos}$ ratios for JaH 422 are still higher than the upper limit given by the model. For DaG 340 the situation is different. The $(^{22}Ne/^{21}Ne)_{cos}$ ratios calculated by using $Ne_{ureilite}$ as a trapped endmember agree to within better than 3% for the three samples, as it is expected considering that all three samples are from the same piece. However, by using Ne_{air} for the component deconvolution, we calculate $(^{22}Ne/^{21}Ne)_{cos}$ ratios of 1.024, 1.198, and 1.228 for the three DaG 340 samples. While the ratios are now within the range defined by the model, the variation of ~20% strongly argues against this procedure. Interestingly, the stepwise heating data for JaH 422 and DaG 340 indicate that both meteorites contain solar cosmic ray (SCR) produced noble gases. The data in the Ne-three-isotope diagram are all close to the cosmogenic endmember but plot distinctly below and to the left of the $Ne_{cos}/Ne_{ureilite}$ and Ne_{cos}/Ne_{air} envelopes (Fig. 3). The existence of solar type gases in DaG 340 has already been demonstrated by Scherer et al. (1998). Solar wind implanted noble gases are usually seen in polymict ureilites, distinguishing them as regolith breccias (e.g., Bischoff et al. 2006; Goodrich et al. 2015). In contrast, JaH 422 and DaG 340 are both classified as main group ureilites. However, DaG 340 might be a clast from a polymict ureilite, considering that many DaG ureilites are polymict.

The CRE ages are determined using the calculated P21 $(^{22}Ne/^{21}Ne)_{cos}$, and $^{21}Ne_{cos}$ values are compiled in Table 4. The ages range from 6.9 Ma for JaH 424 to 36.3 Ma for one of the Kenna samples. The reproducibility of the CRE ages for the two RaS 247 samples is ~10%. Note that this good reproducibility is surprising. The Meteoritical Bulletin lists for RaS 247 a mass of 579 g, which corresponds to a sphere with a radius of ~4 cm. However, in such a small object, we do not expect $(^{22}Ne/^{21}Ne)_{cos}$ or $^{21}Ne_{cos}$ variations in the range 7% or 80%, respectively, as measured by us. With a $(^{22}Ne/^{21}Ne)_{cos}$ ratio as high as 1.202 the preatmospheric radius must have been in the range 10 cm, whereas $(^{22}Ne/^{21}Ne)_{cos} = 1.115$ requires a preatmospheric radius larger than 20 cm. For the following discussion, we use for RaS 247, an (average) CRE age of 24.9 ± 1.2 Ma.

The reproducibility of the seven Kenna samples is not as good as one would like it to be. The ages range between 25.6 and 36.3 Ma, i.e., they vary by ~40%. Since the variation in cosmogenic noble gas concentrations is significantly smaller than the variation in CRE ages, i.e., ~20%, we conclude that a reason for the large scatter is in the highly variable $(^{22}Ne/^{21}Ne)_{cos}$ ratios used to correct for shielding. All our samples come from the same piece of Kenna, i.e., they were less than a few mm apart. We therefore expect very similar shielding conditions and consequently very similar $(^{22}Ne/^{21}Ne)_{cos}$ ratios and $^{21}Ne_{cos}$ concentrations. Indeed, the $^{21}Ne_{cos}$ concentrations vary only by ~20% but the $(^{22}Ne/^{21}Ne)_{cos}$ ratios vary by ~6%, which is substantial and would indicate significant differences in shielding. To be more quantitative, the 6% variation in $(^{22}Ne/^{21}Ne)_{cos}$ results in a more than 40% variation in $^{21}Ne_{cos}$ production rates, which is the reason for the highly variable CRE ages. However, while the reproducibility for the seven samples studied by us is at least reasonable, the CRE ages calculate from the data reported by Okazaki et al. (2003), Rai et al. (2003), and Wilkening and Marti (1976) range from 32.4 to 52.8 Ma, i.e., they vary by more than 60%. By combining all data, the CRE ages for Kenna range from 25.6 to 52.8 Ma, i.e., they vary by more than a factor of 2. Consequently, for reasons not yet understood, the reproducibly of the 11 studied Kenna samples is not satisfying. One might speculate that sample-to-sample heterogeneities might be responsible but it is hard to envision that variations in chemical composition can change the $^{21}Ne_{cos}$ production rates by a factor of two. Note that the measured $^{21}Ne_{cos}$ concentrations of all studied Kenna samples vary by ~70%, which is substantial but which is slightly less than the variations in CRE ages after correcting for shielding using $(^{22}Ne/^{21}Ne)_{cos}$. Therefore, and as already discussed before, some scatter is introduced by the shielding correction because $(^{22}Ne/^{21}Ne)_{cos}$ ratios vary by 6% for the samples studied by us and by about 7% if we also consider the literature data. For the following discussion, we assume for Kenna-a, a CRE age of 35.6 ± 7.4 Ma, which is the average of all 11 individual data.

The CRE age obtained by us for DaG 084 of 16.6 Ma is in reasonable agreement with the CRE age of 18.5 Ma calculated using the data given by Scherer et al. (2000). For the following discussion, we use the average age of 17.5 ± 1.1 Ma. For DaG 319, we can compare our data to the results from Scherer et al. (1998). However, while they found abundant solar type gases, our Ne data are consistent with being a mixture of cosmogenic and $Ne_{ureilite}$, though solar type gases cannot be excluded. The calculated ages are 17.6 Ma for our sample and 21.2 Ma for the samples from Scherer et al. (1998); the grand average value used for further discussion is 19.4 ± 1.8 Ma.

Cosmic Ray Exposure Ages for Ureilites—Easy to Interpret

For discussing literature data, we focus entirely on Ne isotopes because (1) $^{3}He_{cos}$ data are unreliable due to common but highly variable $^{3}He_{cos}$ deficits in most ureilites (see above) and (2) there are not enough data to apply other dating systems like, e.g., ^{36}Cl-^{36}Ar in metal or ^{81}Kr-Kr in bulk samples. By combining our results with literature data, we established a data set comprising 100 data for 41 ureilites, which is the current most complete database for cosmogenic Ne and CRE ages for ureilites. Even more important, our database is the only database that fully considers the shielding dependency of the ^{21}Ne production rates and therefore gives reliable ^{21}Ne CRE ages. The cosmogenic Ne composition for all samples was determined using a two-component deconvolution with the following endmembers: $(^{20}Ne/^{22}Ne)_{cos}$ = 0.8 (Eugster and Michel 1995), $(^{20}Ne/^{22}Ne)_{air}$ = 9.78 and $(^{21}Ne/^{22}Ne)_{air}$ = 0.029 (Meija et al. 2016), $(^{20}Ne/^{22}Ne)_{ureilite}$ = 0.4 and $(^{21}Ne/^{22}Ne)_{ureilite}$ = 0.027 (Ott et al. 1985), and $(^{20}Ne/^{22}Ne)_{solar}$ = 13.75 and $(^{21}Ne/^{22}Ne)_{solar}$ = 0.0333 (Grimberg et al. 2008). Of all analyzed 124 samples, 100 have Ne data that can easily be interpreted as being a mixture of Ne_{cos} with either Ne_{air}, Ne_{solar}, or $Ne_{ureilite}$. In addition, the calculated $(^{22}Ne/^{21}Ne)_{cos}$ ratios for the sample lie within the range allowed by the model predictions, i.e., in the range 1.016–1.235 (see above). The data for 100 samples from 41 ureilites are compiled in Table 4. There we also give the calculated ^{21}Ne production rate and the determined CRE age for each sample. For meteorites where there are more data, we also give the average CRE age together with the standard error of the mean.

Instead of a proper error propagation, which is difficult because sometimes no uncertainties are given for the literature data and error propagation for the component deconvolution is difficult, we assume that the total uncertainty for the CRE ages is entirely dominated by the uncertainties of the model calculations, which is ~15% (see also Fig. 4). We therefore assign an uncertainty of 15% to the individual CRE ages. Note that for establishing a CRE age histogram, the individual uncertainties are not that relevant because the bin sizes are given by statistical constraints and they are usually larger than the uncertainties.

Literature Data—Difficult to Interpret

For some samples from some ureilites, the $(^{22}Ne/^{21}Ne)_{cos}$ ratios are outside the range allowed by the

Table 4. Cosmogenic isotopes, ratios, calculated production rates, and CRE ages for ureilites.

Meteorite name	Reference	DEM	^{21}Ne	^{22}Ne/^{21}Ne	P21	T(^{21}Ne)
Acfer 277	Ott et al. (1993)	Ne-U	0.236	1.135	0.316	0.75
Allan Hills 77257	Ott, personal communication	Ne-U	3.47	1.111	0.352	9.85
Allan Hills 77257	Takaoka (1983)	Ne-U	3.66	1.154	0.287	12.73
Allan Hills 77257	Vogt et al. (1986)	Ne-U	2.84	1.139	0.310	9.16
Allan Hills 77257—Mean						10.6 (1.5)
Allan Hills 78019	Okazaki et al. (2003)	Air	0.36	1.080	0.412	0.87
Allan Hills 78019	Okazaki et al. (2003)	Air	0.37	1.017	0.536	0.69
Allan Hills 78019	Aylmer et al. (1990)		0.03	1.187	0.248	0.12
Allan Hills 78019—Mean						0.56 (0.31)
Allan Hills 81101	Herpers et al. (1995)	Ne-U	5.07	1.130	0.324	15.7
Allan Hills 81101	Ott, personal communication	Ne-U	4.74	1.037	0.464	11.5
Allan Hills 81101	Rai et al. (2003)	Ne-U	4.09	1.088	0.387	10.6
Allan Hills 81101—Mean						12.6 (2.2)
Allan Hills 82106	Ott, personal communication	Ne-U	0.619	1.230	0.173	3.6
Allan Hills 82106	Ott, personal communication	Ne-U	0.610	1.191	0.232	2.6
Allan Hills 82106	Park et al. (2014)	Ne-U	0.759	1.207	0.207	3.7
Allan Hills 82106—Mean						3.3 (0.5)
Allan Hills 82130	Rai et al. (2003)	Air	0.46	1.207	0.217	2.2
Allan Hills 82130-1	Ott, personal communication	Air	0.62	1.191	0.232	2.7
Allan Hills 82130-2	Ott, personal communication	Air	0.61	1.178	0.251	2.4
Allan Hills 82130	Park et al. (2014)	Ne-U	0.82	1.193	0.229	3.6
Allan Hills 82130—Mean						2.7 (0.5)
Allan Hills 84136	Park et al. (2014)	Ne-U	0.78	1.222	0.185	4.2
Almahatta Sitta (AS#36)	Murty et al. (2010)	Ne-U	9.08	1.063	0.425	21.4
Almahatta Sitta (AS#4a)	Welten et al. (2010)	Ne-U	6.93	1.059	0.431	16.1
Almahatta Sitta (AS#4b)	Welten et al. (2010)	Ne-U	7.09	1.056	0.435	16.3
Almahatta Sitta (AS#36)	Welten et al. (2010)	Ne-U	7.25	1.062	0.426	17.0
Almahatta Sitta (AS#44)	Welten et al. (2010)	Ne-U	5.78	1.098	0.372	15.5
Almahatta Sitta (AS#47a)	Welten et al. (2010)	Ne-U	7.66	1.054	0.438	17.5
Almahatta Sitta (AS#47b)	Welten et al. (2010)	Ne-U	8.01	1.036	0.466	17.2
Almahatta Sitta—Mean						17.3 (1.9)
DaG 084	This work	Ne-U	6.44	1.084	0.393	16.6
DaG 084	Scherer et al. (2000)	Ne-U	7.77	1.067	0.419	18.5
DaG 084—Mean						17.5 (1.1)
DaG 319	This work	Ne-U	7.01	1.081	0.400	17.6
DaG 319	Scherer et al. (1998)	Solar	8.04	1.093	0.380	21.2
DaG 319—Mean						19.4 (1.8)
DaG 340 (SWH)	This work	Ne-U	3.368	1.194	0.227	16.2
Dho 132	This work	Ne-U	0.999	1.165	0.271	3.7
Dingo Pup Donga	Bogard et al. (1973)	Ne-U	1.788	1.192	0.230	7.8
Dyalpur	Mazor et al. (1970)	Ne-U	3.50	1.179	0.247	14.2
Dyalpur	Mazor et al. (1970)	Ne-U	4.75	1.225	0.180	26.4
Dyalpur—Mean						20.3 (6.1)
EET 83309	Ott et al. (1993)	Ne-U	15.4	1.106	0.360	42.8
EET 83309	Ott et al. (1993)	Ne-U	12.8	1.124	0.333	38.5
EET 83309	Rai et al. (2003)	Ne-U	19.5	1.124	0.333	58.6
EET 83309	Park et al. (2014)	Ne-U	14.0	1.106	0.360	38.9
EET 83309—Mean						44.7 (8.2)
EET 87511	Park et al. (2014)	Ne-U	1.47	1.152	0.290	5.1
EET 87517	Park et al. (2014)	Ne-U	3.24	1.101	0.367	8.8
EET 87720	Ott et al. (1993)	Solar	2.89	1.119	0.340	8.5
EET 87720	Rai et al. (2003)	Ne-U	3.27	1.126	0.329	9.9
EET 87720	Park et al. (2014)	Ne-U	2.74	1.091	0.383	7.2

Table 4. *Continued*. Cosmogenic isotopes, ratios, calculated production rates, and CRE ages for ureilites.

Meteorite name	Reference	DEM	^{21}Ne	^{22}Ne/^{21}Ne	P21	T(^{21}Ne)
EET 87720—Mean						8.5 (1.1)
Goalpara	Eberhardt and Eberhardt (1960)	Ne-U	8.79	1.122	0.336	26.2
Goalpara	Göbel et al. (1978)	Ne-U	8.30	1.154	0.287	28.9
Goalpara	Mazor et al. (1970)	Ne-U	8.80	1.181	0.247	35.7
Goalpara	Stauffer (1961)	Ne-U	8.55	1.118	0.342	25.0
Goalpara—Mean						28.9 (4.1)
GRA 95205	Park et al. (2014)	Ne-U	4.72	1.079	0.405	11.6
GRA 95205	Park et al. (2014)	Ne-U	3.74	1.090	0.384	9.7
GRA 95205—Mean						10.7 (0.9)
GRA 98032	Park et al. (2014)	Ne-U	6.00	1.210	0.203	29.6
GRA 98032	Park et al. (2014)	Ne-U	5.66	1.214	0.197	28.7
GRA 98032—Mean						29.2 (0.4)
GRO 95575	Park et al. (2014)	Ne-U	2.18	1.094	0.378	5.8
Hajmah (a)	Aylmer et al. (1990)		0.30	1.20	0.22	1.4
HaH 064	Scherer et al. (2000)	Air	0.345	1.224	0.182	1.9
HaH 126	This work	Ne-U	7.733	1.101	0.367	21.0
Haverö	Bogard et al. (1973)	Ne-U	7.86	1.157	0.283	27.8
Haverö	Göbel et al. (1978)	Ne-U	7.98	1.175	0.256	31.2
Haverö	Levsky (1979)	Ne-U	8.55	1.143	0.304	28.1
Haverö	Weber et al. (1971)	Ne-U	7.72	1.185	0.241	32.1
Haverö	Weber et al. (1971)	Ne-U	8.04	1.138	0.312	25.8
Haverö	Rai et al. (2003)	Ne-U	8.09	1.207	0.207	39.0
Haverö	Smith and Fireman (1973)	Ne-U	7.97	1.223	0.183	43.5
Haverö—Mean						32.5 (6.0)
JaH 424	This work	Ne-U	2.676	1.086	0.390	6.9
Kenna-SWH	This work	Ne-U	10.72	1.108	0.357	30.0
Kenna-a	This work	Ne-U	9.51	1.160	0.278	34.2
Kenna-b	This work	Ne-U	10.95	1.110	0.354	30.9
Kenna-c	This work	Ne-U	11.56	1.129	0.325	35.6
Kenna-d	This work	Ne-U	9.63	1.169	0.265	36.3
Kenna-e	This work	Ne-U	10.41	1.109	0.355	29.3
Kenna-f	This work	Ne-U	9.68	1.094	0.378	25.6
Kenna-KP1	Okazaki et al. (2003)	Ne-U	16.30	1.140	0.309	52.8
Kenna-KP2	Okazaki et al. (2003)	Ne-U	13.78	1.133	0.319	43.2
Kenna	Rai et al. (2003)	Ne-U	11.71	1.158	0.281	41.6
Kenna	Wilkening and Marti (1976)	Ne-U	12.94	1.080	0.399	32.4
Kenna—Mean						35.6 (7.4)
LEW 85328	Ott et al. (1993)	Ne-U	4.17	1.130	0.324	12.9
MET 1083	Park et al. (2014)	Ne-U	2.858	1.202	0.215	13.3
MET 1085	Park et al. (2014)	Ne-U	9.45	1.129	0.325	29.1
Nilpena	Ott, personal communication	Air	3.27	1.138	0.312	10.5
Nilpena	Ott, personal communication	Air	4.27	1.130	0.324	13.2
Nilpena	Aylmer et al. (1990)	?	3.78	1.14	0.309	12.3
Nilpena	Rai et al. (2003)	Air	3.42	1.175	0.256	13.4
Nilpena—Mean						12.3 (1.1)
NWA 5928	This work	Ne-U	9.17	1.114	0.348	26.4
Novo-Urei	Eberhardt and Eberhardt (1960)	Ne-U	2.70	1.056	0.435	6.2
Novo-Urei	Göbel et al. (1978)	Ne-U	2.20	1.106	0.360	6.1
Novo-Urei	Mazor et al. (1970)	Ne-U	2.33	1.090	0.384	6.1
Novo-Urei	Stauffer (1961)	Ne-U	2.25	1.088	0.387	5.8
Novo-Urei—Mean						6.1 (0.1)
PCA 82506	Herpers et al. (1995)	Ne-U	1.49	1.194	0.177	8.42
PCA 82506	Ott, personal communication	Ne-U	1.18	1.150	0.273	4.33
PCA 82506—Mean						5.3 (1.3)

Table 4. *Continued*. Cosmogenic isotopes, ratios, calculated production rates, and CRE ages for ureilites.

Meteorite name	Reference	DEM	^{21}Ne	^{22}Ne/^{21}Ne	P21	T(^{21}Ne)
RaS 247-SWH	This work	Ne-U	5.08	1.202	0.215	23.6
RaS 247	This work	Ne-U	9.03	1.115	0.346	26.1
RaS 247—Mean						24.9 (1.2)
RKPA80239	Ott, personal communication	Ne-U	9.21	1.188	0.236	39.0
Roosevelt County 027	Goodrich et al. (1987)	Ne-U	0.62	1.063	0.424	1.5
Roosevelt County 027	Goodrich et al. (1987)	Ne-U	0.89	1.101	0.367	2.4
Roosevelt County 027	Aylmer et al. (1990)	?	0.75	1.08	0.399	1.9
Roosevelt County 027	Wacker (1986)	Ne-U	0.62	1.076	0.405	1.5
RC 027—Mean						1.8 (0.4)
Sahara 98505	Pätsch et al. (2001)	Ne-U	5.53	1.077	0.404	13.7
Yamato-74123	Hintenberger et al. (1978)	Ne-U	1.51	1.231	0.171	8.8
Yamato-74123	Hintenberger et al. (1978)	Ne-U	2.12	1.224	0.182	11.7
Yamato-74123	Hintenberger et al. (1978)	Ne-U	1.41	1.222	0.185	13.0
Yamato-74123—Mean						11.2 (1.8)
Yamato-790981	Ott, personal communication	Ne-U	4.90	1.156	0.284	17.2

Only data with a $(^{22}Ne/^{21}Ne)_{cos}$ ratio that lies within the range of values allowed by the model predictions, i.e., within 1.016–1.235, are included. Abundances are in 10^{-8} cm^3 STP g^{-1} and production rates are in 10^{-8} cm^3 STP g^{-1} Ma^{-1}. The uncertainties for the $^{21}Ne_{cos}$ production rates and therefore for the individual CRE ages are estimated to be ~15%. The given uncertainties for the average values are the 1σ standard deviation of the mean. DEM = deconvolution endmember.

model calculations. This can either be due to unrecognized contributions from solar energetic particles, which are known to increase the $(^{22}Ne/^{21}Ne)_{cos}$ ratios, and/or by the fact that the model predictions for carbonaceous chondrites are not strictly valid for ureilites. For most of the problematic ureilites, there were other samples from the same study or from other studies that could be used to determine the CRE ages. In total, we were unable to calculate CRE ages for the six ureilites, Asuka-881931, EET 83225, FRO 90036, JaH 422, Lahrauli, and North Haig.

The data by Yamamoto et al. (1998) for ALHA77257, Asuka-881931, and Yamato-790981 are not considered because the maximum release temperature of 900 °C used in their study is not sufficient to completely degas ureilite samples and therefore CRE ages determined using their data would be too low. Note that all three ureilites were included in the study by Beard and Swindle (2017). For ALHA78019, the samples measured by Wacker (1986) and Rai et al. (2003) plot outside the $Ne_{cos}/Ne_{ureilite}$ and Ne_{cos}/Ne_{air} envelopes and can therefore not be interpreted as simple two-component mixtures. Sample (b) from Wacker (1986) plots in between the $Ne_{cos}/Ne_{ureilite}$ and Ne_{cos}/Ne_{air} envelopes, suggesting a three-component mixture, while sample (a) plots significantly under both envelopes. The sample reported by Rai et al. (2003) also plots below the Ne_{cos}/Ne_{air} envelope and appears similar to sample (a) studied by Wacker (1986). ALHA78019 likely contains SCR produced Ne but additional data are needed. Wacker (1985) only performed stepwise heating on sample (b) but not on the anomalous sample (a), while the stepwise heating data reported by Rai et al. (2003) are only for temperatures 1000–1600 °C and do not reveal any information about the nontrapped component. For DaG 340, two of the three measured $(^{22}Ne/^{21}Ne)_{cos}$ ratios are slightly higher than allowed by the model, therefore no age can be calculated from them. Only the data obtained from the stepwise heating experiment fall into the allowed range and can be used to determine the CRE age. As a possible explanation why the stepwise heating data seem to be more reliable than the other two data, we might speculate that the stepwise setup possibly better reduces the trapped component, which for DaG 340 is likely solar wind, and therefore provide more reliable cosmogenic data. Rai et al. (2004) analyzed bulk samples and HF/HCl residues for FRO 90036. However, their $(^{22}Ne/^{21}Ne)_{cos}$ ratios after component deconvolution with either Ne_{solar} or $Ne_{ureilite}$ as an endmember is too high, i.e., 2.446 or 1.452, respectively, and therefore no CRE age can be calculated. For JaH 422, all of our $(^{22}Ne/^{21}Ne)_{cos}$ ratios are higher than allowed by the model predictions, clearly indicating the small preatmospheric size of this ureilite and likely indicating that SCRs contribute to the measured Ne budget, which makes the calculation of a CRE age impossible. Note that the small preatmospheric size of JaH 422 is also indicated by its low mass of only 61.6 g (Meteoritical Bulletin). The difficulties for the Kenna data have been discussed before. For the following discussion, we assume for Kenna-a, a CRE age of 35.6 ± 7.4 Ma, which is the average of the seven data measured by us and the four literature data.

The sample of Lahrauli reported by Padia et al. (1983) appears to be almost exclusively cosmogenic, though its $(^{22}Ne/^{21}Ne)_{cos}$ ratio of 1.245 is slightly higher

than the upper limit allowed by the model. In addition, the data reported for this meteorite by Rai et al. (2003) plot below the $Ne_{cos}/Ne_{ureilite}$ and the Ne_{cos}/Ne_{air} envelopes, suggesting the presence of SCR produced Ne. This is further confirmed by the high apparent $(^{22}Ne/^{21}Ne)_{cos}$ ratio of 1.311. Consequently, no age can be calculated for Lahrauli. Beard and Swindle (2017) included Lahrauli in their database despite the possible contributions of SCR Ne. For LEW 85328, only the data by Ott et al. (1993) can be used to determine a CRE age. The $(^{22}Ne/^{21}Ne)_{cos}$ ratio determined from the data by Rai et al. (2003) of 1.327 is higher than allowed by the model predictions.

The sample of Novo-Urei reported by Müller and Zähringer (1969) has a $(^{22}Ne/^{21}Ne)_{cos}$ ratio outside the range allowed by the model predictions. This sample plots well under the $Ne_{cos}/Ne_{ureilite}$ and Ne_{cos}/Ne_{air} envelopes in the Ne-three-isotope diagram. The other four samples of Novo-Urei (Stauffer 1961; Mazor et al. 1970; Göbel et al. 1978; Aylmer et al. 1990) can well be explained as simple mixing between Ne_{cos} and $Ne_{ureilite}$ and all have consistent CRE ages. Therefore, either some error was made while measuring the Müller and Zähringer (1969) sample or that particular sample somehow differed significantly from the other three. For Yamato-74123, all measured samples (Hintenberger et al. 1978; Ott, personal communication; Aylmer et al. 1990) give $(^{22}Ne/^{21}Ne)_{cos}$ ratios higher than allowed by the model; consequently no CRE age can be calculated. The $(^{22}Ne/^{21}Ne)_{cos}$ ratio of 1.284 for EET 83225 determined from the data by Park et al. (2014) is also higher than the range predicted by the model calculations, therefore no CRE age can be calculated. Finally, the data for North Haig (e.g., Bogard et al. 1973) indicate significant $^{21}Ne_{cos}$ losses and can therefore not be used to calculate a CRE age (Aylmer et al. 1990). Note that both EET 83225 and North Haig were included in the study by Beard and Swindle (2017).

COSMIC RAY EXPOSURE HISTOGRAM

The CRE ages calculated here are based on our current best knowledge on shielding corrected ^{21}Ne production rates. In this respect, our study differs from the two earlier approaches by Herzog and Caffee (2014) and Park et al. (2014), both of which used a constant and therefore shielding independent ^{21}Ne production rate of 0.412×10^{-8} cm^3 STP g^{-1} Ma^{-1}. Beard and Swindle (2017) also used a constant ^{21}Ne production rate, which was calculated from the data for the lunar surface (Hohenberg et al. 1978) multiplied by a factor of two to account for a 4π exposure geometry. The ^{21}Ne production rates used by us vary between 0.171×10^{-8} cm^3 STP g^{-1} Ma^{-1} for one Yamato-74123 sample and 0.493×10^{-8} cm^3 STP g^{-1} Ma^{-1} for one sample of ALHA78019, i.e., the ^{21}Ne production rates vary by a factor of almost three. The average of all ^{21}Ne production rates used by us is 0.316×10^{-8} cm^3 STP g^{-1} Ma^{-1}, i.e., about 30% lower than the (average) production rate used by Herzog and Caffee (2014) and Park et al. (2014).

Considering the data for Kenna, for which the shielding correction increased the scatter of the CRE ages (see above), it is reasonable to ask if the shielding correction is necessary and if so if it is reliable. Considering the first point (necessity), we argue that using a constant $^{21}Ne_{cos}$ production rate might distort the CRE age histogram. In contrast, it is obvious that using shielding corrected $^{21}Ne_{cos}$ production rates, if properly done, is beneficial and cannot have any negative effects. Therefore, if possible, a shielding correction should always be performed. Considering the second point (reliability), we checked the data by investigating if there is a correlation between CRE ages and ^{21}Ne production rates (Table 4). The argument is as follows, a false correction for shielding can produce too low or too high ^{21}Ne production rates for certain $(^{22}Ne/^{21}Ne)_{cos}$ ratios, i.e., for certain shielding conditions. In such a case, there could be a (false) correlation between ^{21}Ne production rates and $(^{22}Ne/^{21}Ne)_{cos}$ ratios. We find no correlation between ^{21}Ne production rates and CRE ages, clearly indicating the reliability of our data compilation.

The histogram of ^{21}Ne CRE ages for both updated literature data and our newly reported data are shown in the upper panel of Fig. 5. The CRE ages for ALHA82106 and ALHA82130 of 3.3 ± 0.5 and 2.7 ± 0.5 Ma confirm the pairing of the ALH82xxx ureilites (e.g., Mason 1985; Takeda et al. 1988). Since there are no indications for further paring, we assume that our database contains 40 individual ureilite falls. Based on the CRE age data available at that time, Goodrich (1992) and Scherer et al. (1998) stated that there was no apparent clustering of CRE ages. Later and based on a larger data set, Herzog and Caffee (2014) argued for a broad maximum between 9 and 25 Ma (~40% of all ureilites). According to them, there is also a possible peak near 10 Ma and they concluded that at least three events produced the known ureilites (Fig. 5, middle panel). By adding 13 new CRE ages to the database, Park et al. (2014) essentially confirmed the findings by Herzog and Caffee (2014). In contrast, Beard and Swindle (2017) argued for CRE age clusters at <1 Ma, ~1 Ma, ~2–3 Ma, ~4–5 Ma, ~9 Ma, and ~20 Ma, though it is not clear how some of the clusters could be separated considering the uncertainties involved calculating the CRE ages (Fig. 5 lower panel).

The CRE age histogram showing the database established by us (Fig. 5 upper panel) indicates that 11 out of the 40 studied ureilites have ^{21}Ne CRE ages of less than or equal to 5.8 Ma; five ureilites have unusually low CRE ages of even less than 2 Ma (Acfer 277, ALHA78019, Hajmah, HaH 064, RC 027). ALHA78019 has a CRE age of 560 kyr, which is in the range typical for CM chondrites and lunar meteorites (cf, Herzog and Caffee 2014). The longest CRE age is ~45 Ma (EET 83309). Interpreting the CRE age histogram is not without problems. With a spread of almost 45 Ma for the CRE ages and a bin size for the histogram of 2.5 Ma, there are on average 2.2 meteorites per bin, which is not sufficient to clearly resolve detailed structures. From the limited data, we can conclude that there is no apparent clustering in the CRE age histogram, except for a slight indication of a peak in the range 30 Ma. There is a trend, however, of decreasing meteorite number with increasing CRE age, the trend is roughly exponential. There are more ureilites with short CRE ages than there are ureilites with long exposure ages. This is also obvious considering that the range of CRE ages is ~44 Ma but the median of the data is ~12.5 Ma. One could argue, however, that there is a peak in the range 30 Ma, which will be discussed further below.

Also the two histograms by Herzog and Caffee (2014) (Fig. 5 middle panel) and Beard and Swindle (2017) (Fig. 5 lower panel) show a decrease in the CRE age histogram. However, while the CRE age histogram by Herzog and Caffee (2014) is somewhat uncertain due to the relatively low number of meteorites, the CRE age distribution by Beard and Swindle (2017) seems steeper than the one established by us and the one published by Herzog and Caffee (2014). The differences are likely due to the choice of the used ^{21}Ne production rates. By way of example, the longest CRE age determined by us is for EET 83309. The ^{21}Ne production rate used by us for this meteorite is 0.347×10^{-8} cm^3 STP g^{-1} Ma^{-1}, which is 20% lower than the 0.421×10^{-8} cm^3 STP g^{-1} Ma^{-1} used by Herzog and Caffee (2014) and therefore results in a 20% higher CRE age. Another interesting example is for one of the Haverö data (Smith and Fireman 1973). From the $(^{22}Ne/^{21}Ne)_{cos}$ ratio of 1.223, we calculate a $^{21}Ne_{cos}$ production rate of 0.183, i.e., more than a factor of two lower than the production rate used by Herzog and Caffee (2014). Consequently, while we calculate with our approach for Haverö a CRE age of 43.5 Ma (Table 4), we would calculate a CRE age of about 19 Ma using the $^{21}Ne_{cos}$ production rate from Herzog and Caffee (2014). Since most of the production rates used by us are slightly lower than the average production rates used in the two other studies, we calculate on average slightly higher CRE ages, which naturally produces a less steep decrease in the CRE age distribution.

For the (roughly) exponential behavior of the CRE age histogram, we can find two possible explanations. First, it might be that meteorite delivery from the UDBs is actually increasing, i.e., that currently more ureilites are produced and delivered to Earth than in the past. This, in combination with a constant destruction rate of the ureilites, would naturally produce a decreasing behavior in the CRE age histogram. Higher meteorite delivery rates can be due to higher collision rates inside the asteroid belt or at least in the orbital

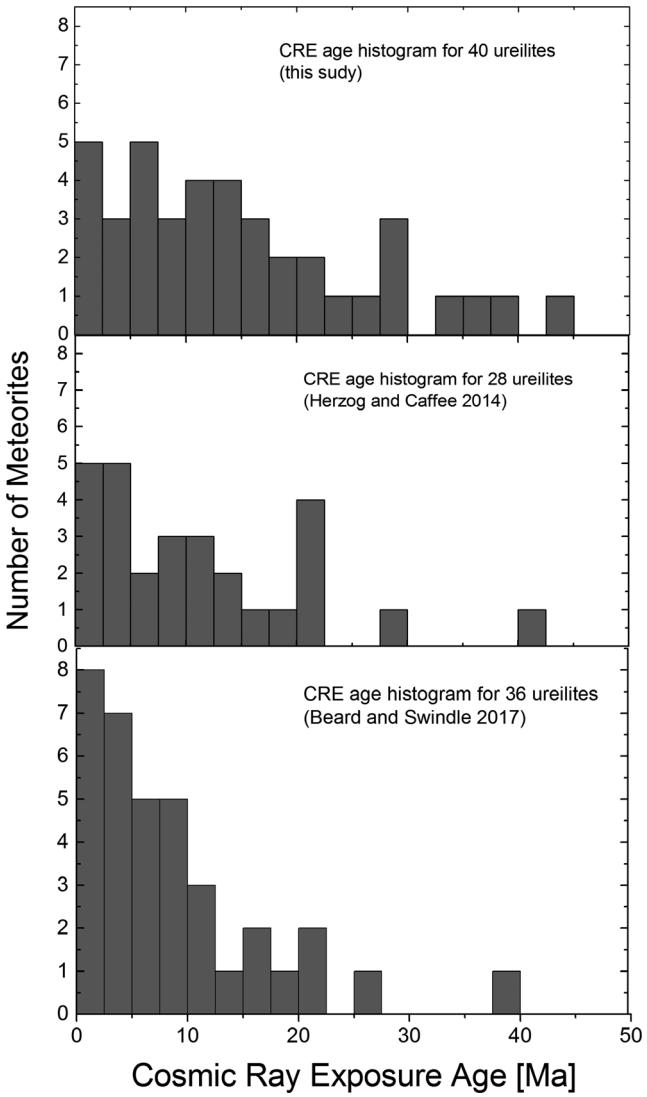

Fig. 5. (Pairing corrected) cosmic ray exposure histogram for ureilites. The upper panel shows the results from our study, the middle panel shows the results from Herzog and Caffee (2014), and the lower panel shows the results from Beard and Swindle (2017). All three CRE age histograms show a decreasing number of ureilites with increasing CRE age.

region of the UDB. We consider higher collision rates unlikely because this would also be seen in other meteorite groups. It could be possible, however, that the orbit of the UDB somehow differ from the orbits of the other meteorite parent bodies and that higher collision rates only occur in this special region of the asteroid belt. Another possibility is that the collisions that produce meteoroids are now taking place at locations closer to a resonance. A UDB that slowly moves closer to an effective resonance while suffering impacts at a constant rate would naturally produce meteorites with shorter and shorter CRE ages and therefore a CRE age histogram as seen in Fig. 5. It has been speculated that the UDB is located in the Nysa-Polana region, which is within about 0.1 AU of the 3:1 resonance (e.g., Gayon-Markt et al. 2012). If true, the UDB is indeed, at least currently, located close to a very effective resonance.

A second possibility is that meteorite delivery from the UDB is temporarily constant but that some type of loss mechanism reduces the lifetime of the ureilites. As loss mechanisms one can imagine erosion, collisions, or loss of ureilites either into the Sun or onto other solar system planets. A similar scenario has been proposed by Takeda et al. (1988), who argued that ureilites were created early in the solar system and that rapid erosion in space accounts for the absence of ureilites with long exposure ages. If erosion were the main loss mechanism, one would expect that all ureilites are affected to the same or at least similar degrees. By assuming constant erosion rates, meteorites with short CRE ages would have preatmospheric radii very close to their radii at ejection from the UDB because erosion has not yet reduced their dimensions. On the other hand, meteorites having a large preatmospheric radius must have short CRE ages because they are still large. However, the data indicate differently. The large ureilites ALHA81101, DaG 084, and Almahata Sitta with $(^{22}Ne/^{21}Ne)_{cos}$ ratios lower than or equal to 1.067 all have CRE ages in the range 10–20 Ma, i.e., not exceptionally short. Though, we cannot exclude that some of the large ureilites from our collections were produced even much larger and entered Earth atmosphere still large, i.e., erosion indeed reduced the size of the original meteoroid but even after CRE the meteoroid was still large, we would nevertheless expect some kind of relationship between CRE age and preatmospheric radius. We therefore conclude that the data contradict the hypothesis that erosion is the main loss mechanism. This result confirms earlier studies on erosion rates (e.g., Schaeffer et al. 1981). If meteorite breakup would be the most relevant loss mechanism, we can essentially follow the same arguments as before for the case of erosion; large objects must have short CRE ages because they have not yet been broken into smaller pieces. Since this is not what is seen in the data, we can exclude breakup as a relevant loss mechanism shaping the CRE age histogram of ureilites. On the other hand, a *meteorite loss* that is independent on meteorite size, i.e., small and large ureilites are lost at a very similar rate, into the Sun, onto other solar system planets or out of the solar system would naturally produce a CRE age histogram as seen in Fig 5.

To summarize, a likely explanation for the overall structure of the CRE age histogram for ureilites, i.e., the decreasing number of ureilites with increasing CRE age, is to imagine either that the UDB actually moves closer to the meteorite delivering resonance and/or that there is an effective type of loss mechanism. Either effects, or a combination of the two, would naturally produce more ureilites with short CRE ages, exactly what is seen in Fig. 5.

Using our model predictions tailored for ureilites and assuming ~85% atmospheric ablation losses, we find that $(^{22}Ne/^{21}Ne)_{cos}$ ratios higher or equal to 1.10 most likely indicate preatmospheric radii less or equal 20 cm, which can be considered as small. With the database from Table 4, we find that 28 out of the 40 studied ureilites, i.e., almost 70%, had preatmospheric radii less than 20 cm. This finding confirms earlier less quantitative results by Aylmer et al. (1990) and Park et al. (2014). A possible explanation as to why a large number of ureilites, at least from the ones studied by us, have small preatmospheric radii is that they are all derived from the UDB, which is composed of re-accreted material from the original ureilite parent body (e.g., Downes et al. 2008; Herrin et al. 2010a, 2010b; Goodrich et al. 2015). Impacts on such a brecciated asteroid would naturally produce small meteoroids, most likely in the size range of the clasts in the breccia. Note that the largest sizes of clasts from the Almahata Sitta fall were all in the range 200–300 g (e.g., Herrin et al. 2010b), which corresponds to a radius of about 3 cm, i.e., even smaller than the radii calculated by us.

The CRE age histogram showing the new data (Fig. 5, upper panel) depicts what might be a peak at ~30 Ma. The possible peak consists of the three ureilites Goalpara (28.9 Ma), GRA 98032 (29.2 Ma), and MET 1085 (29.1 Ma). We can also add NWA 5928 and Haverö with CRE ages of 26.4 and 32.5 Ma, respectively, to the list. We can now ask ourselves whether the five ureilites have other features in common. The forsterite numbers of Goalpara, GRA 98032, and Haverö are all in a narrow range between 78.6 and 79.0, i.e., they indicate a similar petrologic origin of the samples (cf. Beard and Swindle 2017). Unfortunately, there are no data for the other two ureilites MET 1085 and NWA 5928. The conclusion that can be drawn, however, is not very significant because there is a large peak in the distribution of olivine core

compositions around Fo 79-81 (Goodrich et al. 2015) and the finding that the five ureilites all have Fo number in that range is therefore not surprising. Although the result is compromised by the low statistic, we suggest that a big impact on the UDB ~30 Ma ago produced the three (or five) homogeneous ureilites.

SUMMARY

We measured the noble gas isotopic concentrations of He, Ne, and Ar for 21 samples from the 10 ureilites, DaG 084, DaG 319, DaG 340, Dho 132, HaH 126, JaH 422, JaH 424, Kenna, NWA 5928, and RaS 247, using both single and stepwise heating extractions. Here we report the CRE ages. By also considering literature data, we compiled a consistent set of CRE ages for ureilites. All CRE ages were calculated using production rates for cosmogenic ^{21}Ne by fully considering their dependence on preatmospheric radius and shielding depth (Leya and Masarik 2009). In this respect, our study is more advanced than earlier studies, which are based on a constant, i.e., shielding independent, ^{21}Ne production rate (e.g., Herzog and Caffee 2014; Park et al. 2014; Beard and Swindle 2017).

The CRE age histogram is now based on 100 samples from 40 different ureilites. The result is surprising: The number of meteorites decreases with increasing CRE age, i.e., there are more ureilites with short CRE ages than there are ureilites with long CRE ages. As a possible explanation, we speculate that either the parent body of the known ureilites is currently moving closer to a resonance and/or that there is some loss mechanism involved, which affects all ureilites the same, i.e., the loss mechanism is independent on the size of the meteorite. In addition and superimposed to the finding that the number of ureilites is decreasing with increasing CRE age, there is a slight indication for a peak in the range 30 Ma, which contains up to 12% of the studied ureilites. Finally, we confirm earlier results (Aylmer et al. 1990; Park et al. 2014) that the majority of the studied ureilites have relatively small preatmospheric radii, i.e., they have preatmospheric radii less than or equal to ~20 cm.

Acknowledgments—We thank M. Cosarinsky, U. Calmonte, and R. Trappitsch for their assistance in preparing and measuring some of the samples, and P. Enderli and H.-E. Jenni for their tireless work at keeping the mass spectrometer laboratory working. We are very grateful to the reviewers—an anonymous reviewer, G. Herzog, H. Downes, and C. Goodrich who all helped us in improving the paper. The ureilite samples for DaG 319, DaG 340, JaH 422, JaH 424, and RaS 247 were all kindly provided by B. Hofmann from the Natural History Museum in Bern. Sample NWA 5928, which is so far the only ureilite from the NWA collection studied for noble gases, was gratefully provided by T. Jakubowski. We also thank O. Volk for his assistance in translating the Levsky (1979) paper from the original Russian. This work was supported by the Swiss National Science Foundation (200021_159562).

Editorial Handling—Dr. Cyrena Goodrich

REFERENCES

Alexeev V. A. 1998. Parent bodies of L and H chondrites: Times of catastrophic events. *Meteoritics & Planetary Science* 33:145–152.

Amelin Y., Koefoed P., Bischoff A., Budde G., Brennecka G., and Kleine T. 2015. Pb isotopic age of ALM-A—A feldspar-rich volcanic rock from the crust of the ureilite parent body. 78th Annular Meeting of the Meteoritical Society, LPI contribution 1856.

Aylmer D., Vogt S., Herzog G. F., Klein J., Fink D., and Middleton R. 1990. Low ^{10}Be and ^{26}Al contents of ureilites: Production at meteoroid surfaces. *Geochimica et Cosmochimica Acta* 54:1775–1784.

Beard S. P. and Swindle T. D. 2017. Search for evidence of source event grouping among ureilites. *Meteoritics & Planetary Science* 11:2343–2352.

Bhandari N., Shah V. G., and Graham A. 1981. The Lahrauli ureilite. *Meteoritics* 16:185–191.

Bischoff A., Scott E. R. D., Metzler K., and Goodrich C. A. 2006. Nature and origins of meteoritic breccias. In *Meteorites and the early solar system II*, edited by Lauretta D. S. and McSween H. Y. Jr. Tucson, Arizona: The University of Arizona Press. pp. 679–714.

Bogard D. D., Gibson E. K., Moore D. R., Turner N. L., and Wilkin R. B. 1973. Noble gas and carbon abundances of the Haverö, Dingo Pup Donga, and North Haig ureilites. *Geochimica et Cosmochimica Acta* 37:547–557.

Boynton W. V., Starzyk P. M., and Schmitt R. A. 1976. Chemical evidence for the genesis of the ureilites, the achondrite Chassigny and the nakhlites. *Geochimica et Cosmochimica Acta* 40:1439–1447.

Busemann H., Baur H., and Wieler R. 2000. Primordial noble gases in "phase Q" in carbonaceous and ordinary chondrites studied by closed-system stepped etching. *Meteoritics & Planetary Sciences* 35:949–973.

Clayton R. N. and Mayeda T. K. 1988. Formation of ureilites by nebular processes. *Geochimica et Cosmochimica Acta* 52:1313–1318.

Cosarinsky M., Calmonte U., Hofmann B., and Leya I. 2010. Noble gas data on ureilites from the Lybian, Omani, and Moroccan deserts (abstract #1770). 41st Lunar and Planetary Science Conference. CD-ROM.

Downes H., Mittlefehldt D. W., Noriko K., and Valley J. W. 2008. Evidence from polymict ureilite meteorites for a disrupted and re-accreted single ureilite parent asteroid gardened by several distinct impactors. *Geochimica et Cosmochimica Acta* 72:4825–4844.

Eberhardt P. and Eberhardt A. 1960. Neon und andere Edelgase in Steinmeteoriten. *Helvetica Physica Acta* 33:593–594.

Eugster O. 1988. Cosmic-ray production rates for ^{3}He, ^{21}Ne, ^{38}Ar, ^{83}Kr, and ^{126}Xe in chondrites based on ^{81}Kr-Kr exposure ages. *Geochimica et Cosmochimica Acta* 52:1649–1662.

Eugster O. and Michel T. 1995. Common asteroid break-up events of eucrites, diogenites, and howardites and cosmic-ray production rates for noble gases in achondrites. *Geochimica et Cosmochimica Acta* 59:177–199.

Friedrich J. M., Wolf S. F., Rumble D., Troiano J., Gagnon C. J. L., Compton J. R., Jenniskens P., and Shaddad M. H. 2010. The elemental composition of Almahatta Sitta. *Meteoritics & Planetary Science* 45:1718–1727.

Gayon-Markt J., Delbo M., Morbidelli A., and Marchi S. 2012. On the origin of the Almahata Sitta meteorite and 2008 TC3 asteroid. *Monthly Notices of the Royal Astronomical Society* 424:508–518.

Göbel R., Ott U., and Begemann F. 1978. On trapped noble gases in ureilites. *Journal of Geophysical Research: Solid Earth* 83:855–867.

Goodrich C. A. 1992. Ureilites: A critical review. *Meteoritics* 27:327–352.

Goodrich C. A., Keil K., Berkley J., Laul J. C., Smith M. R., Wacker J. F., Clayton R. N., and Mayeda T. K. 1987. Roosevelt County 027: A low-shock ureilite with interstitial silicates and high noble gas concentrations. *Meteoritics* 22:191–218.

Goodrich C. A., Scott E. R. D., and Fioretti A. M. 2004. Ureilitic breccias: Clues to the petrologic structure and impact disruption of the ureilite asteroid. *Chemie der Erde* 64:283–327.

Goodrich C. A., Hutcheon I. D., Kita N. T., Huss G. R., Cohen B. A., and Keil K. 2010. ^{53}Mn-^{53}Cr and ^{26}Al-^{26}Mg ages of a feldspathic lithology in polymict ureilites. *Earth and Planetary Science Letters* 295:531–540.

Goodrich C. A., Hartmann W. K., O'Brian D. P., Weidenschilling S. J., Wilson L., Michel P., and Jutzi M. 2015. Origin and history of ureilitc material in the solar system: The view from asteroid 2008 TV3 and the Almahata Sitta meteorite. *Meteoritics & Planetary Science* 50:782–809.

Grimberg A., Baur H., Bühler F., Bochsler P., and Wieler R. 2008. Solar wind helium, neon, and argon isotopic and elemental composition: Data from the metallic glass flown on NASA's Genesis mission. *Geochimica et Cosmochimica Acta* 72:626–645.

Herpers U., Vogt S., Bremer K., Hofmann H., Suter M., Wieler R., Lange H., and Michel R. 1995. Cosmogenic nuclides in differentiated antarctic meteorites: Measurements and model calculations. *Planetary and Space Science* 43:545–556.

Herrin J. S., Zolensky M. E., Michael E., Ito M., Le L., Mittlefehldt D. W., Jenniskens P., Ross A. J., and Shaddad M. H. 2010a. Thermal and fragmentation history of ureilitic asteroids: Insights from the Almahata Sitta fall. *Meteoritics & Planetary Science* 45:1789–1803.

Herrin J. S., Ito M., Zolensky M. E., Mittlefehldt D. M., Jenniskens P. M., and Shaddad M. H. 2010b. Thermal and fragmentation of the ureilitic asteroids: Insights from the Almahata Sitta fall (abstract #1095). 41st Lunar and Planetary Science Conference.

Herzog G. F. and Caffee M. W. 2014. Cosmic-ray exposure ages of meteorites. In *Treatise on geochemistry*, 2nd ed., edited by Holland H. and Turekian K. Oxford: Newnes. pp. 419–454.

Hintenberger H., Jochum K., Braun O., Christ P., and Martin W. 1978. The Antarctic meteorite Yamato-74123—A new ureilite. *Earth and Planetary Science Letters* 40:187–193.

Hohenberg C. M., Marti K., Podosek F. A., Reedy R. C., and Shirck J. R. 1978. Comparison between observed and predicted cosmogenic noble gases in lunar samples. Proceedings, 9th Lunar and Planetary Science Conference. pp. 2311–2344.

Huber L., Gnos E., Hofmann B., Welten K. C., Nishizumi K., Caffee M. W., Hillegonds D. J., and Leya I. 2008. The complex exposure history of the Jiddat al Harasis 073 L-chondrite shower. *Meteoritics & Planetary Science* 43:1691–1708.

Janssens M.-J., Hertogen J., Wolf R., Ebihara M., and Anders E. 1987. Ureilites: Trace element clues to their origin. *Geochimica et Cosmochimica Acta* 51:2275–2283.

Janots E., Gnos E., Hofmann B. A., Greenwood R. C., Franchi I. A., and Bischoff A. 2011. Jiddat al Harasis 422: A ureilite with an extremely high degree of shock melting. *Meteoritics & Planetary Science* 46:134–148.

Jaques A. L. and Fitzgerald M. J. 1982. The Nilpena ureilite, an unusual polymict breccia: Implications for origin. *Geochimica et Cosmochimica Acta* 46:893–900.

Jarosewich E. 1990. Chemical analyses of meteorites: A compilation of stony and iron meteorite analyses. *Meteoritics* 25:323–337.

Levsky L. K. 1979. Rare gases in carbonaceous chondrites. *Meteoritika* 38:27–36.

Leya I. and Masarik J. 2009. Cosmogenic nuclides in stony meteorites revisited. *Meteoritics & Planetary Science* 44:1061–1086.

Mason B. 1985. *Antarctic Meteorite Newsletter* 8:42.

Mazor E., Heymann D., and Anders E. 1970. Noble gases in carbonaceous chondrites. *Geochimica et Cosmochimica Acta* 34:781–824.

McCall G. J. H. and Cleverly W. H. 1968. New stony meteorite finds including two ureilites from the Nullarbor Plain, Western Australia. *Mineralogical Magazine* 36:691–716.

Meija J., Coplen T. B., Berglund M., Brand W. A., De Bièvre P., Gröning M., Holden N. E., Irrgeher J., Loss R. D., Walczyk T., and Prohaska T. 2016. Isotopic compositions of the elements 2013 (IUPAC Technical Report). *Pure and Applied Chemistry* 88:293–306.

Mittlefehldt D. W., McCoy T. J., Goodrich C. A., and Kracher A. 1998. Non-chondritic meteorites from asteroidal bodies. In *Planetary materials*, edited by Papike J. J. Reviews in Mineralogy, vol. 35. Washington, D.C.: Mineralogical Society of America. pp. 4-001–4-196.

Müller O. and Zähringer J. 1969. Rare gases in stony meteorites. In *Meteorite research*, edited by Millman P. M. Dordrecht: Reidel. pp. 845–865.

Murty S. V. S., Mahajan R. R., Jenniskens P., Shaddad M. H., and Eldien B. 2010. Noble gases and nitrogen in the Almahata Sitta ureilite. *Meteoritics & Planetary Science* 45:1751–1764.

Nishiizumi K., Regnier S., and Marti K. 1980. Cosmic ray exposure ages of chondrites, pre-irradiation and constancy of cosmic ray flux in the past. *Earth and Planetary Science Letters* 50:156–170.

Okazaki R., Nakamura T., Takaoka N., and Nagao K. 2003. Noble gases in ureilites released by crushing. *Meteoritics & Planetary Science* 38:767–781.

Ott U., Löhr H. P., and Begemann F. 1985. Trapped neon in ureilites—A new component. *Rapports isotopiques dans le systeme solaire (Isotopic ratios in the solar system)*, edited by Gautier D. Paris: Centre National d'Etudes Spatiales. pp. 129–136.

Ott U., Löhr H. P., and Begemann F. 1993. Solar noble gases in polymict ureilites and an update on ureilite noble gas data (abstract). *Meteoritics* 28:415–416.

Padia J. T., Rao M. N., Venkatesan T. R., and Bhandari N. 1983. Noble gases in Lahrauli ureilite (abstract). *Meteoritics* 18:369.

Park J., Herzog G. F., Haba M. K., and Nagao K. 2014. Exposure ages of ureilites: Radionuclides and noble gases (abstract #1618). 45th Lunar and Planetary Science Conference. CD-ROM.

Pätsch M., Weber H. W., and Schultz L. 2001. Noble gas investigations of new meteorites from Africa (abstract #1526). 32nd Lunar and Planetary Science Conference. CD-ROM.

Rai V. K., Murty S. V. S., and Ott U. 2003. Noble gases in ureilites: Cosmogenic, radiogenic, and trapped components. *Geochimica et Cosmochimica Acta* 67:4435–4456.

Rai V. K., Murty S. V. S., and Ott U. 2004. Nitrogen and noble gases in two monomict ureilites Acfer 277 and FRO90036 from hot and cold deserts (abstract #1180). 35th Lunar and Planetary Science Conference. CD-ROM.

Sanders I., Scott E., and Delaney J. 2017. Origin of mass-independent oxygen isotope variation among ureilites: Clues from chondrites and primitive achondrites. *Meteoritics & Planetary Science* 52:690–708.

Schaeffer O. A., Nagel K., Fechtig H., and Neukum G. 1981. Space erosion of meteorites and secular variation of cosmic rays (over 10^9 years). *Planetary and Space Science* 29:1109–1118.

Scherer P., Zipfel J., and Schultz L. 1998. Noble gases in two new ureilites from the Saharan desert (abstract #1383). 29th Lunar and Planetary Science Conference. CD-ROM.

Scherer P., Päetsch M., and Schultz L. 2000. Noble gases in 15 meteorites from the Sahara: Eucrites, ureilites, and ordinary chondrites. In *Workshop on Extraterrestrial Materials from Cold and Hot Deserts*, edited by Schultz L., Franchi I. A., Reid A. M., and Zolensky M. E. Houston, Texas: Lunar and Planetary Institute. pp. 72–75.

Schwarzmüller J. 1971. Ein Edelgasanalysensystem mit automatischer Datenerfassung und Edelgasmessungen an Strukturelementen des Apollo 11 Mondstaubes. Ph.D. thesis, University of Bern, Bern, Switzerland.

Smith S. and Fireman E. 1973. Ages of eight recently fallen meteorites. *Journal of Geophysical Research* 78:3249–3259.

Stauffer H. 1961. Primordial argon and neon in carbonaceous chondrites and ureilites. *Geochimica et Cosmochimica Acta* 24:70–82.

Takaoka N. 1983. Noble gases in ALH-77257 ureilite (abstract). *Papers presented to the Eighth Symposium on Antarctic Meteorites*. pp. 81–82.

Takeda H. 1987. Mineralogy of Antarctic ureilites and a working hypothesis for their origin and evolution. *Earth and Planetary Science Letters* 81:358–370.

Takeda H., Mori H., and Ogata H. 1988. On the pairing of Antarctic ureilites with reference to their parent body. *Proceedings of the NIPR Symposium on Antarctic Meteorites* 1:145–172.

Vdovykin G. P. 1976. The Haverö meteorite. *Space Science Reviews* 18:749–776.

Vogt S., Herpers U., Sarafin R., Signer P., Wieler R., Suter M., and Woelfli W. 1986. Cosmic ray records in Antarctic meteorites. In *International workshop on Antarctic meteorites*, edited by Annexstad J. O., Schultz L., and Wänke H. Houston, Texas: Lunar and Planetary Institute. pp. 55–57.

Wacker J. 1986. Noble gases in the diamond-free ureilite, ALHA78019: The roles of shock and nebular processes. *Geochimica et Cosmochimica Acta* 50:633–642.

Warren P. H. 2012. Parent body depth-pressure temperature relationships and the style of the ureilite anataxis. *Meteoritics & Planetary Science* 47:209–227.

Warren P. and Kallemeyn G. 1989. Geochemistry of polymict ureilite EET83309, and a partially-disruptive impact model for ureilite origin. *Meteoritics* 24:233–246.

Weber H. W., Hintenberger H., and Begemann F. 1971. Noble gases in the Haverö ureilite. *Earth and Planetary Science Letters* 13:205–209.

Welten K. C., Caffee M. W., Leya I., Masarik J., Nishiizumi K., and Wieler R. 2003. Noble gases and cosmogenic radionuclides in the Gold Basin L4 chondrite shower: Thermal history, exposure history, and pre-atmospheric size. *Meteoritics & Planetary Science* 38:157–173.

Welten K. C., Meier M. M. M., Caffee M. W., Nishiizumi K., Wieler R., Jenniskens P., and Shaddad M. H. 2010. Cosmogenic nuclides in Almahata Sitta ureilites: Cosmic-ray exposure age, preatmospheric mass, and bulk density of asteroid 2008 TC_3. *Meteoritics & Planetary Science* 45:1728–1742.

Wiik H. B. 1969. On regular discontinuities in the composition of meteorites. *Commentationes Physico-Mathematicae* 34:135–145.

Wiik H. B. 1972. The chemical composition of the Haverö meteorite and the genesis of the ureilites. *Meteoritics* 7:553–557.

Wilkening L. and Marti K. 1976. Rare gases and fossil particle tracks in the Kenna ureilite. *Geochimica et Cosmochimica Acta* 40:1465–1473.

Wilson L., Goodrich C. A., and Van Orman J. 2008. Thermal evolution and physics of melt extraction of the ureilite parent body. *Geochimica et Cosmochimica Acta* 72:6154–6176.

Yamamoto T., Hashizume K., Matsuda J., and Kase T. 1998. Multiple nitrogen isotopic components coexisting in ureilites. *Meteoritics & Planetary Science* 33:857–870.

Yanai K., Kojima H., and Haramura H. 1995. *Catalog of the Antarctic Meteorites collected from December 1969 to December 1994, with special reference to those represented in the collections of the National Institute of Polar Research*. Tokyo: National Institute of Polar Research. pp. 44–76, 212–213.